Evolution of the magnetotail energetic-electron population during high-speed-stream-driven storms: Evidence for the leakage of the outer electron radiation belt into the Earth's magnetotail

Joseph E. Borovsky[1,2] and Michael H. Denton[3,4]

Received 1 April 2011; revised 10 October 2011; accepted 11 October 2011; published 28 December 2011.

[1] For 15 high-speed-stream-driven geomagnetic activations (weak storms) in 2006–2007, the temporal behaviors of the outer electron radiation belt at geosynchronous orbit and the energetic-electron population of the magnetotail are compared via superposed-epoch averaging of data. The magnetotail measurements are obtained by using GPS-orbit measurements that magnetically map out into the magnetotail. Four temporal phases of high-speed-stream-driven storms are studied: (1) the pre-storm density decay of the electron-radiation belt, (2) the electron-radiation-belt density dropout near the time of storm onset, (3) the rapid density recovery a few hours after dropout, and (4) the heating of the electron radiation belt during the high-speed-stream-driven geomagnetic activity. In all four phases the behaviors of the outer electron radiation belt and of the energetic-electron population in the magnetotail are the same and simultaneous. The physical explanations for the behavior in phase 1 (decay), phase 2 (dropout), and phase 4 (heating) lie in the dipolar regions of the magnetosphere: hence for those three phases it is concluded that the temporal behavior of the energetic-electron population in the magnetotail mimics the behavior of the outer electron radiation belt. Behavior attributable to physical processes in the dipole is seen in the magnetotail energetic-electron population: this implies that the origin of the energetic-electron population of the magnetotail is "leakage" or "outward evaporation" from the outer electron radiation belt in the dipolar magnetosphere.

Citation: Borovsky, J. E., and M. H. Denton (2011), Evolution of the magnetotail energetic-electron population during high-speed-stream-driven storms: Evidence for the leakage of the outer electron radiation belt into the Earth's magnetotail, *J. Geophys. Res.*, *116*, A12228, doi:10.1029/2011JA016713.

1. Introduction

[2] The outer electron radiation belt has been studied for decades [*Vernov et al.*, 1959; *Dessler and Karplus*, 1960; *Hess and Poirier*, 1962; *Friedel et al.*, 2002; *Hudson et al.*, 2008; *Miyoshi and Kataoka*, 2011]. A density-temperature description of the outer electron radiation belt finds that the density of the outer electron radiation belt is $\sim 5 \times 10^{-4}$ cm^{-3} at geosynchronous orbit and the temperature is ~150 keV at geosynchronous orbit [*Cayton et al.*, 1989; *Denton et al.*, 2010]. This radiation-belt electron population is separate from the suprathermal electron population of the electron plasma sheet, which has a temperature ~30 keV at geosynchronous orbit [*Cayton et al.*, 1989; *Denton et al.*, 2010]. The density-and-temperature description of the electron radiation belt has been found to be very compact and insightful. Basically the density n is a measure of the number of radiation-belt electrons and the temperature T is a measure of the hardness of the spectrum; nT is a measure of the energy density (kinetic pressure) and $T/n^{2/3}$ is the density of electron adiabatic invariants per unit flux.

[3] The energetic-electron population of the Earth's magnetotail has also been studied for decades [*Montgomery et al.*, 1965; *Vernov et al.*, 1969; *Retzler and Simpson*, 1969; *Sarris et al.*, 1976; *Meng et al.*, 1981; *Taylor et al.*, 2004; *Sergeev et al.*, 2008], but it is less studied than the outer electron radiation belt of the dipolar magnetosphere. A density-temperature description finds that it has a number density $\sim 2 \times 10^{-4}$ cm^{-3} and a temperature ~100 keV [*Denton and Cayton*, 2011].

[4] By statistically matching relativistic specific entropies, *Borovsky and Cayton* [2011] found evidence that the outer electron radiation belt at geosynchronous orbit and the energetic-electron population of the magnetotail are the same population. That conclusion was also made by *Taylor et al.* [2004] based on energetic-electron phase-space density measured at geosynchronous orbit and in the magnetotail. The implication of this sameness is that either (a) the magnetotail energetic-electron population is the source population of the outer electron radiation belt or (b) that the energetic-electron population of the magnetotail is owed to outward leakage (evaporation) of the outer electron radiation belt. In case (a) the question is then what is the source

[1]Los Alamos National Laboratory, Los Alamos, New Mexico, USA.
[2]AOSS, University of Michigan, Ann Arbor, Michigan, USA.
[3]Physics Department, Lancaster University, Lancaster, UK.
[4]Space Science Institute, Boulder, Colorado, USA.

0148-0227/11/2011JA016713

Table 1. Summary of the Conclusions Drawn From Observations

Phase of Storm	Phase Observed Both at Geosynchronous Orbit and in the Magnetotail?	Location of Physical Cause	Conclusion
Density Decay	Yes	Dipole	Tail energetic electrons mimic the dipole radiation belt
Density Dropout	Yes	Dipole	Tail energetic electrons mimic the dipole radiation belt
Density Recovery	Yes	Unknown	None
Heating	Yes	Dipole	Tail energetic electrons mimic the dipole radiation belt

population of the magnetotail energetic-electron population: in case (b) the question is then what is the source population of the outer electron radiation belt.

[5] Three outstanding questions about these energetic-electron populations in the Earth's magnetosphere are the following. (1) What is the source population of the outer electron radiation belt? (2) What is the origin of the energetic-electron population in the magnetotail? (3) Is there transport of energetic electrons between the radiation belt, the outer magnetosphere, and the magnetotail?

[6] For clues about these three questions, this study will compare the temporal evolution of the outer electron radiation belt in the dipole and the energetic-electron population in the magnetotail. This evolution will be compared for the same geomagnetic events using superposed-epoch analysis. These events will be weak high-speed-stream-driven storms.

[7] The response of the outer electron radiation belt to high-speed-stream-driven storms has been extensively studied in recent years [cf. *Tsurutani et al.*, 2006; *Borovsky and Denton*, 2006; *Denton et al.*, 2008, 2009; *Kavanagh and Denton*, 2007; *McPherron et al.*, 2009; *Morley*, 2010]. During high-speed-stream-driven storms the outer electron radiation belt undergoes a characteristic pattern of evolution involving the following four phases. (1) The radiation-belt number density decays exponentially in the days prior to storm onset owing to a buildup of the outer plasmasphere during the "calm before the storm" [*Borovsky and Steinberg*, 2006; *Borovsky and Denton*, 2009a]. (2) The radiation-belt number density drops dramatically near the time of storm onset [*Borovsky et al.*, 1998a; *Denton et al.*, 2010; *Borovsky and Denton*, 2009b, 2010b]. (3) The radiation-belt number density rapidly recovers to a new level several hours after the density dropout [*Borovsky et al.*, 1998a; *Denton et al.*, 2010; *Borovsky and Denton*, 2010b]. (4) The temperature of the outer electron radiation belt increases steadily at about 35 keV per day during the high speed stream that drives the geomagnetic storm [*Denton et al.*, 2010; *Borovsky and Denton*, 2010b]. It is this heating in phase 4 that can give rise to the exceptionally high fluxes of MeV electrons that are famously known as "killer electrons" [*Graham*, 1994].

[8] This manuscript is organized as follows. In section 2 the spacecraft measurements and event selection are discussed, as is the magnetic mapping between the GPS orbit and the magnetotail. In section 3 the evolution of the outer electron radiation belt at geosynchronous orbit during the high-speed-stream-driven geomagnetic activations is studied and in section 4 the evolution of the energetic-electron population in the magnetotail is studied during the same high-speed-stream-driven geomagnetic activations. In section 5 conclusions are drawn from the observations and the conclusions are collected into Table 1. The results are summarized in section 6, and section 7 contains a discussion comparing the present conclusions to the results of previous studies.

2. Data Sets, Data Analysis, and Event Selection

[9] Measurements of energetic electrons from two sets of spacecraft will be analyzed: (1) equatorial measurements from the Synchronous Orbit Particle Analyzer (SOPA) onboard 7 satellites in geosynchronous orbit (6.6 R_E) will be used to determine the properties of the outer electron radiation belt and (2) high-latitude measurements from the Burst Detection Dosimeter (BDD-IIR) and the Combined X-ray and Dosimeter (CXD) onboard 12 Global Positioning System (GPS) satellites will be used to determine the properties of the energetic-electron population in the magnetotail.

2.1. Measurements of the Outer Electron Radiation Belt

[10] The energetic electrons at geosynchronous orbit are measured by the Synchronous Orbit Particle Analyzer (SOPA) [*Belian et al.*, 1992; *Cayton and Belian*, 2007] onboard 7 satellites in geosynchronous orbit (6.6 R_E). The SOPAs measure fluxes of electrons in the energy range ~30 keV to >2 MeV every 10 s. In the current study a relativistic-Maxwellian electron distribution function is fit to the measurements of the outer electron radiation belt. The spin-averaged counting rates for each electron energy channel are modeled as linear combinations of two Maxwellian components plus a non-electron "background" contribution; minimizing the squared deviations between the observed and model counting rates summed over 10 electron channels yields the best fit two-Maxwellian spectra (see *Cayton and Belian* [2007] for full details). *Cayton et al.* [1989] found that relativistic bi-Maxwellians were excellent fits to the omnidirectional electron fluxes at geosynchronous orbit; *Pierrard and Lemaire* [1996] drew similar conclusions for the outer electron radiation belt away from geosynchronous orbit. The assumption of isotropy is implicit in the present data analysis; future analysis will produce densities and temperatures of the electron bi-Maxwellians as functions of pitch angle. A recent survey [*Borovsky and Denton*, 2011] of the anisotropy of the outer electron radiation belt at geosynchronous orbit found that whereas electrons with energies greater than 1 MeV can exhibit high anisotropies [cf. *Kaye et al.*, 1978; *Selesnick and Blake*, 2002; *Fritz et al.*, 2003], the bulk of the outer electron radiation belt with energies of 100–200 keV is quasi-isotropic at geosynchronous orbit [cf. *Borovsky and Denton*, 2011, Figures 2 and 6]. The bi-Maxwellian fitting describes two populations of electrons: a "soft" population of electrons with a temperature of ~30 keV and a "hard" population of electrons with a temperature of ~150 keV [*Cayton et al.*, 1989; *Denton et al.*,

2010]. The "soft" population is the suprathermal tail of the electron plasma sheet whose appearance at geosynchronous orbit is associated with substorm injections [*Lezniak et al.*, 1968; *Cayton et al.*, 1989; *Birn et al.*, 1998, 2000]. The hard component is the outer electron radiation belt [*Cayton et al.*, 1989; *Belian et al.*, 1996; *Borovsky and Denton*, 2010b].

[11] With the 10-s cadence of the SOPA-measured electron count rates, the temperature and density of the outer electron radiation belt are determined every 10 s from each geosynchronous satellite. To reduce the influence of outliers when the fits are noisy and to produce a more-manageable-sized data set, median values of the density and temperature are calculated for every 30 min of data [cf. *Denton et al.*, 2010] and those 30-min median values are used. Data from the years 2006 and 2007 (where there is temporal overlap with processed GPS data) will be the focus of the present study.

[12] When directly comparing the temporal behavior of the outer electron radiation belt at geosynchronous orbit to the behavior of the energetic-electron population of the magnetotail, only geosynchronous-orbit measurements within ±1 h of local midnight will be used.

2.2. Measurements of the Energetic-Electron Population in the Magnetotail

[13] Omnidirectional energetic-electron measurements in the energy range ~100 keV–6 MeV on 12 Global Positioning System (GPS) satellites are used to determine the number density and temperature of the energetic-electron population in the Earth's magnetotail. The measurements used in this report are from the years 2006 and 2007 (where there is temporal overlap with available geosynchronous data). The instrumentation used is the Burst Detection Dosimeter (BDD-IIR) [*Cayton et al.*, 1998, 2010] operating on two early satellites and the Combined X-ray and Dosimeter (CXD) [*Distel et al.*, 1999; *Cayton et al.*, 2010] instruments operating on 10 later satellites, with modeling of the instrument response by *Tuszewski et al.* [2002]. Densities and temperatures of the electrons are obtained from relativistic-Maxwellian fits to the electron count rates [cf. *Denton and Cayton*, 2011]. The count rate corrected for dead time is modeled as a sum of two contributions: non-electron background counts plus counts that result from a distribution of incident electrons. Values for the density and temperature of the electrons are inferred by least squares fits of relativistic Maxwellians, minimizing the sum of the squared deviations between the sets of true and predicted counting rates. The analysis is optimized for the energies ~100 keV–1.0 MeV.

[14] The energetic-electron population in the magnetotail will be measured from high-latitude nightside portions of the GPS orbits. The methodology is similar to the use of low-altitude measurements to sample the magnetotail ion plasma sheet by the DMSP spacecraft [*Wing and Newell*, 1998] or by the Aureol-3 satellite [*Stepanova et al.*, 2008], but using higher-altitude GPS-orbit measurements. In general the energetic-electron population in the magnetotail is quasi-isotropic [*Hones et al.*, 1968; *Retzler and Simpson*, 1969; *Sarris et al.*, 1976], so the population is easily detected by the off-equatorial GPS spacecraft and Liouville's theorem preserves the number density and the temperature of the energetic-electron population along the flux tube away from the equator. Note that the portion of the magnetotail pitch angle distribution sampled by GPS is the portion with equatorial pitch angles near zero. Mapping of the magnetic field lines from the GPS spacecraft to the equatorial (minimum-B) plane is performed with the T89 [*Tsyganenko*, 1989; *Peredo et al.*, 1993] magnetic field model using an IGRF internal field [see also *Denton and Cayton*, 2011]. The Kp value for the T89 model is set to Kp = 2. The T89 magnetic field model is known to be inaccurate in the magnetotail near local midnight [cf. *Borovsky et al.*, 1998b; *Pulkkinen and Tsyganenko*, 1996], but mapping with the model is only used to indicate magnetic field lines that go into the magnetotail and into the deeper magnetotail. Using the magnetic field models the value B_{sat} of the magnetic field at the GPS satellite is estimated. Computationally tracing the magnetic field line through the satellite, the bounce invariant $\int(1 - B/B_{sat})^{1/2}$ ds is integrated for a particle mirroring at the satellite. Using the asymptotic expansion of *Hilton* [1971], an approximate value for McIlwain's L parameter [*McIlwain*, 1961] is obtained. This L parameter is used as a measure of the downtail distance that the GPS satellite maps to. Only GPS measurements that map to greater than 10 R_E downtail (L > 10) are used and only GPS measurements made within ±1 h of local midnight are used.

2.3. Errors in the Density-Temperature Fits

[15] A systematic study of the errors in the density-temperature fits for the SOPA and GPS data sets has not been undertaken. Some sources of errors [cf. *Cayton and Belian*, 2007] are (a) uncertainties in the instrument response functions, (b) errors in the count rates owing to telemetry glitches, (c) low count rates during density dropouts, and (d) non-Maxwellian distribution functions. The latter source of error is known to be systematic on the GPS orbits for L < 6, which are excluded from the L > 10 data set utilized in the present study.

2.4. Event Selection: Weak High-Speed-Stream-Driven Storms

[16] For overlap between the two data sets (geosynchronous and GPS), high-speed-stream-driven geomagnetic activations in the two years 2006 and 2007 are chosen. These activations are not as strong nor as long-lasting as the high-speed-stream-driven storms of 1993–1995 and 2003–2005 used in previous radiation belt studies [*Borovsky and Denton*, 2009b; *Denton et al.*, 2010; *Borovsky and Denton*, 2010b], but the radiation belt shows the same sequence of evolution as in the stronger storms (see section 1), and indeed the radiation belt at geosynchronous orbit is as intense during these weaker activations as the belt during strong high-speed-stream-driven storms.

[17] The events are selected by examining solar wind velocity measurements and the Kp index. 27-day-repeating high-speed streams that have sustained geomagnetic activations are chosen. (The high-speed stream must show 27-day repeating, the activation need not show 27-day repeating.) For the two years 2006–2007, 22 such events are found. For the present study, data will be superposed for averaging and the superposition will be triggered on rapid recoveries from the density dropouts of the electron radiation belt at geosynchronous orbit. Of the 22 events, 15 are found

to have rapid density recoveries from dropouts. (3 events showed very weak dropouts and 4 events had insufficient geosynchronous data to discern the time of recovery from dropout.) These 15 events are used for the present study.

[18] In Figure 1 the superposed median values of the solar wind velocity (Figure 1a), the superposed average of the Kp index (Figure 1b), the superposed averages of Dst and Dst* (Figure 1c), and the superposed median of the solar wind number density are plotted for the 15 activations, with the zero epoch being the electron-radiation-belt number-density recovery from dropout at geosynchronous orbit. The plots extend from 3 days prior to radiation-belt density recovery to 4 days after radiation-belt density recovery. As can be seen in Figure 1a, the events are associated with fast solar wind following slow wind, with an expected corotating interaction region in the slow-to-fast-wind transition. Unlike the high-speed-stream-driven storms studied previously where fast wind was sustained for several days [cf. *Denton and Borovsky*, 2008, Figure 1; *Borovsky and Denton*, 2010b, Figure 4], the fast solar wind for the present events lasts only 2 or 3 days. As can be seen in Figure 1b, the geomagnetic activations are of relatively short duration compared with the high-speed-stream-driven storms studied previously (compare with *Denton and Borovsky* [2008, Figure 2] or *Borovsky and Denton* [2010b, Figure 4]). Note in the superposed average of Kp in Figure 1b the distinct "calm before the storm" where geomagnetic activity is anomalously low prior to the onset of activity. During these calms, the outer plasmasphere will build up to high density out to geosynchronous orbit and beyond [*Borovsky and Steinberg*, 2006; *Denton and Borovsky*, 2008; *Borovsky and Denton*, 2009a]. In Figure 1c the Dst index (solid curve) and Dst* curve (dashed curve) are plotted. In Figure 1d a greatly increased solar wind number density just prior to recovery from radiation-belt density dropout is seen. This increased solar wind number density is the cause of the radiation-belt dropout (either by compression of the dayside magnetosphere causing radiation-belt electrons to drift to the dayside magnetopause or by production of a superdense plasma sheet which drives enhanced plasma-wave scattering of radiation-belt electrons into the atmosphere). This enhanced solar wind density is associated with compressed slow wind in the CIR at the slow-fast wind transition [*Gosling et al.*, 1978; *Richter and Luttrell*, 1986; cf. *Borovsky and Denton*, 2010c, Figure 4].

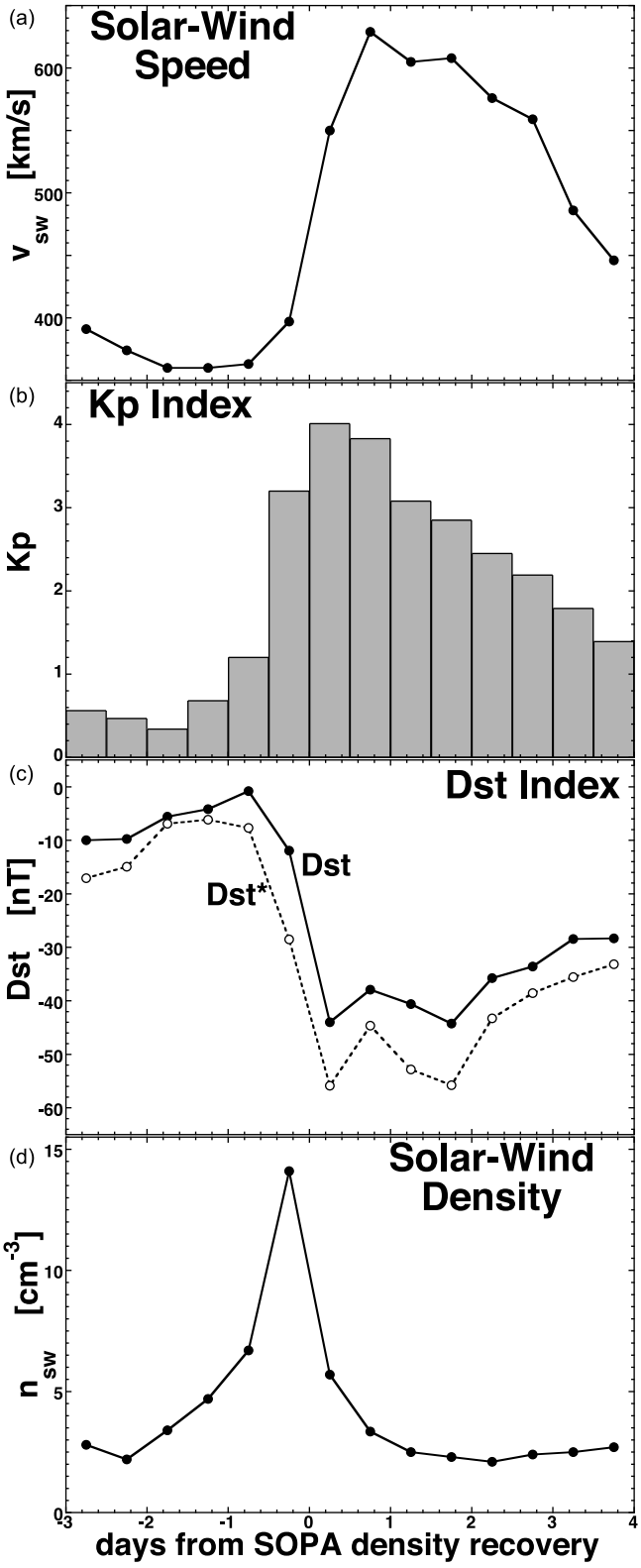

3. Evolution of the Outer Electron Radiation Belt During the High-Speed-Stream-Driven Activations

[19] This section is divided into two subsections. In the first subsection the evolution of the outer electron radiation belt at geosynchronous orbit is examined for the high-speed-stream-driven geomagnetic activations (weak storms) of 2006–2007. It will be found that the evolution during these high-speed-stream-driven weak storms is essentially the same as the behavior during strong high-speed-stream-driven storms. In the second subsection the physical processes acting in the dipolar (middle) magnetosphere that drive that evolution are discussed.

Figure 1. For the 15 high-speed-stream-driven weak storms of 2006 and 2007, (a) the superposed average of the solar wind speed, (b) the superposed average of the Kp index, (c) the superposed averages of Dst and Dst*, and (d) the superposed average of the solar wind number density are plotted as functions of time. The zero epoch in the horizontal axis is the time of sudden recovery of the number density of the outer electron radiation belt at geosynchronous orbit.

3.1. Observations of the Electron-Radiation-Belt Behavior

[20] In Figure 2 the superposed averages of the logarithm of the outer electron radiation belt number density at geosynchronous orbit (Figure 2a), the logarithm of the outer electron radiation belt temperature at geosynchronous orbit (Figure 2b), and the logarithm of the 1.1–1.5 MeV omnidirectional electron flux (Figure 2c) are plotted. The horizontal axis is time in days from the density recovery of the outer electron radiation belt and the vertical axis is the local time around geosynchronous orbit at which the measurement is made. The plots extend from 5 days prior to density recovery to 7 days after recovery.

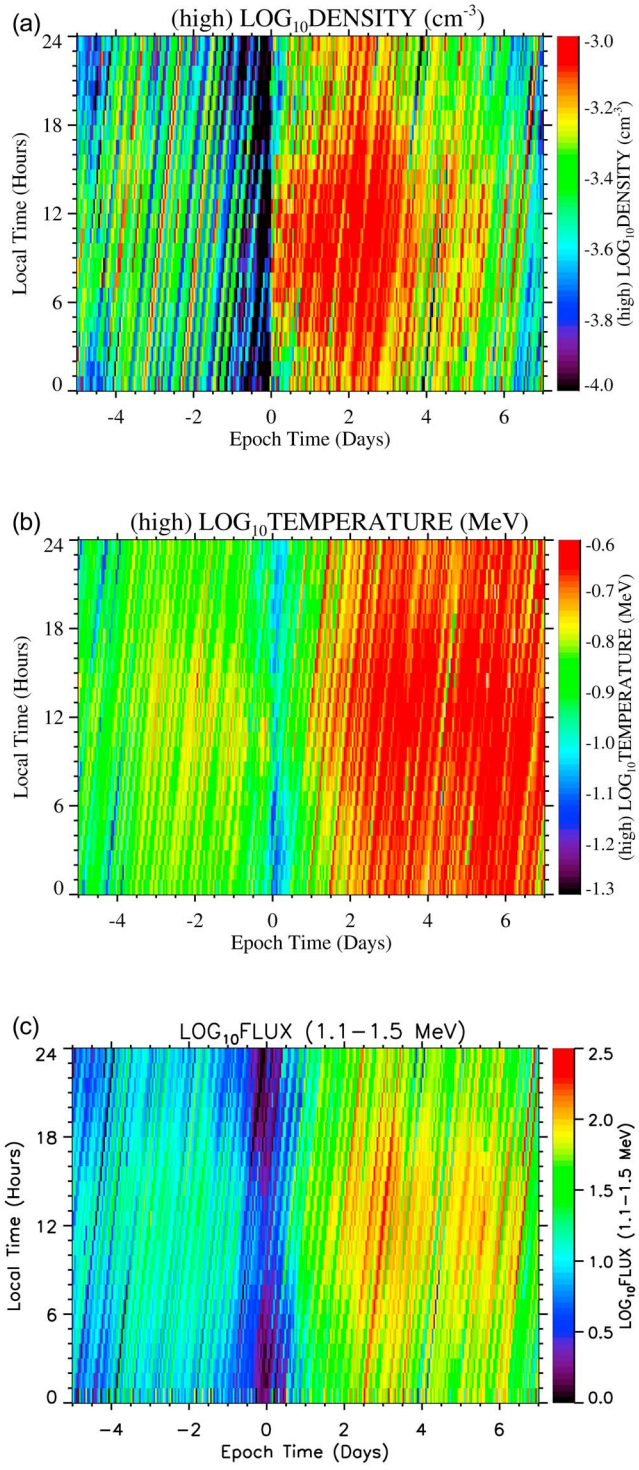

Figure 2. For the 15 high-speed-stream-driven weak storms of 2006 and 2007, (a) the superposed average of the logarithm of the outer electron radiation belt number density at geosynchronous orbit, (b) the superposed average of the logarithm of the outer electron radiation belt temperature at geosynchronous orbit, and (c) the superposed average of the logarithm of the 1.1–1.5 MeV omnidirectional electron flux at geosynchronous orbit are plotted as functions of time (horizontal axis) and local time (vertical axis). The zero epoch in the horizontal axis is the time of sudden recovery of the number density of the outer electron radiation belt at geosynchronous orbit.

[21] In Figure 2a it is seen that the number density of the outer electron radiation belt decreases with time in the days prior to density recovery. This decrease occurs at all local times. A study of high-speed-stream-driven storms has indicated that the decrease is only present when there is a calm before the storm, wherein the outer plasmasphere fills [*Borovsky and Denton*, 2009a; *Denton et al.*, 2010]. At time t = 0 in Figure 2a the number density is seen to rapidly increase at all local times. At local noon the increase is the most rapid. For each event, the zero epoch is chosen as the time at which the first geosynchronous-orbit spacecraft experiences density recovery. The density recovery is sharpest at local noon in Figure 2: this indicates that the density recovery tends to happen first at local noon. After the density recovery, the number density is approximately constant with time at all local times for a few days. Note a general trend in Figure 2a is that the number density of the outer electron radiation belt at geosynchronous orbit tends to be highest at local noon and lowest at local midnight: this is owed to the fact that geosynchronous local noon samples a deeper outer-electron-radiation-belt population (with a higher n and higher T) than does geosynchronous-orbit midnight [cf. *Hones*, 1963; *Roederer*, 1967; *Pfitzer et al.*, 1969; *Borovsky and Denton*, 2010b].

[22] In Figure 2b it is seen that the temperature of the outer electron radiation belt at geosynchronous orbit is approximately constant with time in the days before activity onset while the number density is decreasing with time. Note in Figure 2b that when the number density of the outer electron radiation belt recovers after dropout, the temperature of the outer electron radiation belt is relatively cool and that its temperature increases slowly and steadily during the high-speed-stream-driven geomagnetic activation after recovery. This heating occurs at all local times. The temperature increases for about 2 or three days after onset, then remains approximately constant thereafter; the temporally increasing temperature $\partial T/\partial t$ is positive during the interval of fast wind and geomagnetic activity (cf. Figure 1) and is near zero afterward. Note also in Figure 2c the general trend that at any time the outer electron radiation belt at geosynchronous orbit is hottest at local noon and coolest at local midnight.

[23] In Figure 2c it is seen that the flux of 1.1–1.5 MeV relativistic electrons decreases slowly with time during the calm before the storm before time t = 0 (as the number density

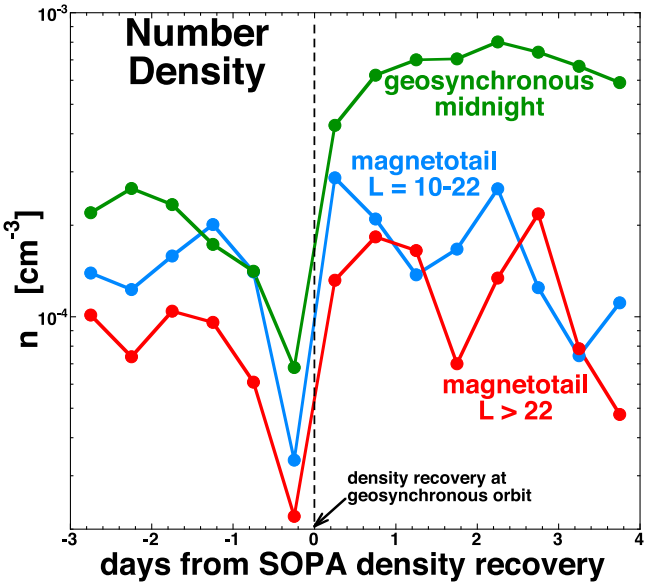

Figure 3. For the 15 high-speed-stream-driven weak storms of 2006 and 2007, the superposed logarithmic average of the energetic-electron number density is plotted as a function of time. The green curve is for the outer electron radiation belt at geosynchronous-orbit local midnight, the blue curve is for the near-Earth magnetotail, and the red curve is for the more-distant magnetotail. The zero epoch in the horizontal axis is the time of sudden recovery of the number density of the outer electron radiation belt at geosynchronous orbit.

of the outer electron radiation belt decreases slowly with time in Figure 2a). After time t = 0 when the number density recovers (Figure 2a), note a slower recovery of the relativistic-electron fluxes occurs (Figure 2c). This slow recovery of relativistic-electron flux is controlled more by the temperature increase of the outer electron radiation belt than by the density of electrons. And as can be seen in Figure 2c, the flux of relativistic electrons slowly increases in the days after t = 0 as the outer electron radiation belt is heated at constant density. Note in Figure 2c that the peak of the 1.1–1.5 MeV electron flux occurs about 2 days into the geomagnetic activity (at t ~ 2 day). For the stronger high-speed-stream-driven storms this peak is usually a few days after storm onset [e.g., *Nagai*, 1988; *Baker et al.*, 1990; *Borovsky et al.*, 1998a; cf. *McPherron et al.*, 2009, Figure 9; *Denton et al.*, 2010, Figure 7]; for the weak high-speed-stream-driven storm studied here the earlier peaking is probably owed to the shorter duration of the fast wind (Figure 1a) and the shorter duration of the geomagnetic activation (Figure 1b) which leads to a shorter interval of heating $\partial T/\partial t$ (Figure 2b).

[24] In Figures 3, 5, and 6 line plots of the number density n, temperature T, and specific entropy S of the outer electron radiation belt at geosynchronous-orbit local midnight are plotted. In Figure 3 the superposed logarithmic average of the number density n at local midnight is plotted (green curve). From day −2.25 to −0,75 the number density decays during the calm before the storm. An exponential fit to n(t) yields a exponential-decay rate of 2.3 days: this is comparable to the 3.4-day exponential decay rate measured prior to high-speed-stream-driven storms by *Borovsky and Denton* [2009a]. Note that the green curve in Figure 3 shows a distinct number density drop in the half day prior to the t = 0 density recovery: this is the density dropout of the outer electron radiation belt at about the time of onset of the geomagnetic activation. Time t = 0 was chosen to be the time of rapid density recovery of the outer electron radiation belt so there is a strong increase in density from the point before t = 0 to the point after t = 0. Note in the days after recovery that the number density of the outer electron radiation belt is approximately constant [see also *Borovsky et al.*, 1998a; *Borovsky and Denton*, 2010b].

[25] To assess the robustness of the superposed averaging, the number density of the electron radiation belt at local midnight is plotted in Figure 4 (top), where the logarithmic average is plotted as the curve with points and the upper and lower quartiles are plotted as the curves without points. As can be seen, the trend indicated by the logarithmic mean is also indicated by the upper quartile and the lower quartile, indicating that the trend is quite robust.

[26] In Figure 5 the temperature T of the outer electron radiation belt at geosynchronous-orbit midnight is plotted as the green curve. Prior to dropout as the number density decays, the temperature of the outer electron radiation belt is approximately constant with time [see also *Borovsky and Denton*, 2009a, 2010b]. During the density dropout (first point before t = 0 in Figure 5) the temperature decreases, but owing to the low density the temperature determination may not be accurate. When the number density returns (first data point after t = 0) the outer electron radiation belt is cool (~100 keV) and afterwards the outer electron radiation belt heats steadily during the geomagnetic activity. The averaged daily heating rate of the green curve of Figure 5 in the time t = 1 day to t = 4 day is 30 keV per day for the outer electron radiation belt at local-midnight geosynchronous orbit. This compares with a heating rate of about 29 keV per day measured by *Borovsky and Denton* [2010b] for geosynchronous-orbit midnight during high-speed-stream-driven storms, which had higher levels of geomagnetic activity than do the 2006–2007 high-speed-stream-driven activations of the present study.

[27] In Figure 6 the specific entropy S of the outer electron radiation belt at geosynchronous-orbit local midnight is plotted as the green curve. Nonrelativistically the specific entropy (entropy per unit mass) is $S = T/n^{2/3}$ [*Bernstein et al.*, 1958; *Birn and Schindler*, 1983; *Goertz and Baumjohann*, 1991]. For a relativistic Maxwellian distribution of particles, *Borovsky and Cayton* [2011] derived the relativistic specific entropy to be

$$S_{rel} = \{(\alpha/K_2(\alpha))\exp[-\alpha K_3(\alpha)/K_2(\alpha)]\}^{-2/3} n^{-2/3} \qquad (1)$$

where $\alpha = m_e c^2/k_B T$ and where K_2 and K_3 are modified Bessell functions. Borovsky and Cayton showed that the specific entropy of expression (1) can be well approximated as

$$S_{rel} \approx T\left(1 + (T/137.9)^{1.275}\right)^{1/1.275} n^{-2/3}, \qquad (2)$$

which is an ~49% increase over the expression $T/n^{2/3}$ at T = 100 keV and an ~80% increase over the expression $T/n^{2/3}$ at T = 150 keV. Note that utilizing specific entropy only makes sense for a population of particles that "stay together." Radiation-belt electrons are magnetically tied to a drift shell,

so in a fluid sense the electrons stay co-located. In the magnetotail the energetic electrons are not trapped, but they are probably slowly drifting and so this co-location argument works to a degree. As can be seen in Figure 6, the specific entropy of the outer electron radiation belt at geosynchronous orbit increases slowly during the calm before the storm owing to the decay in number density at constant temperature [cf. *Borovsky and Denton*, 2009a, Figure 5], the specific entropy greatly increases during the radiation-belt density dropout just before t = 0, the specific entropy greatly drops as the radiation-belt density recovers just after t = 0, and the specific entropy slowly increases in the days after t = 0 as the radiation belt is heated at constant number density [cf. *Borovsky and Denton*, 2010b, Figure 3].

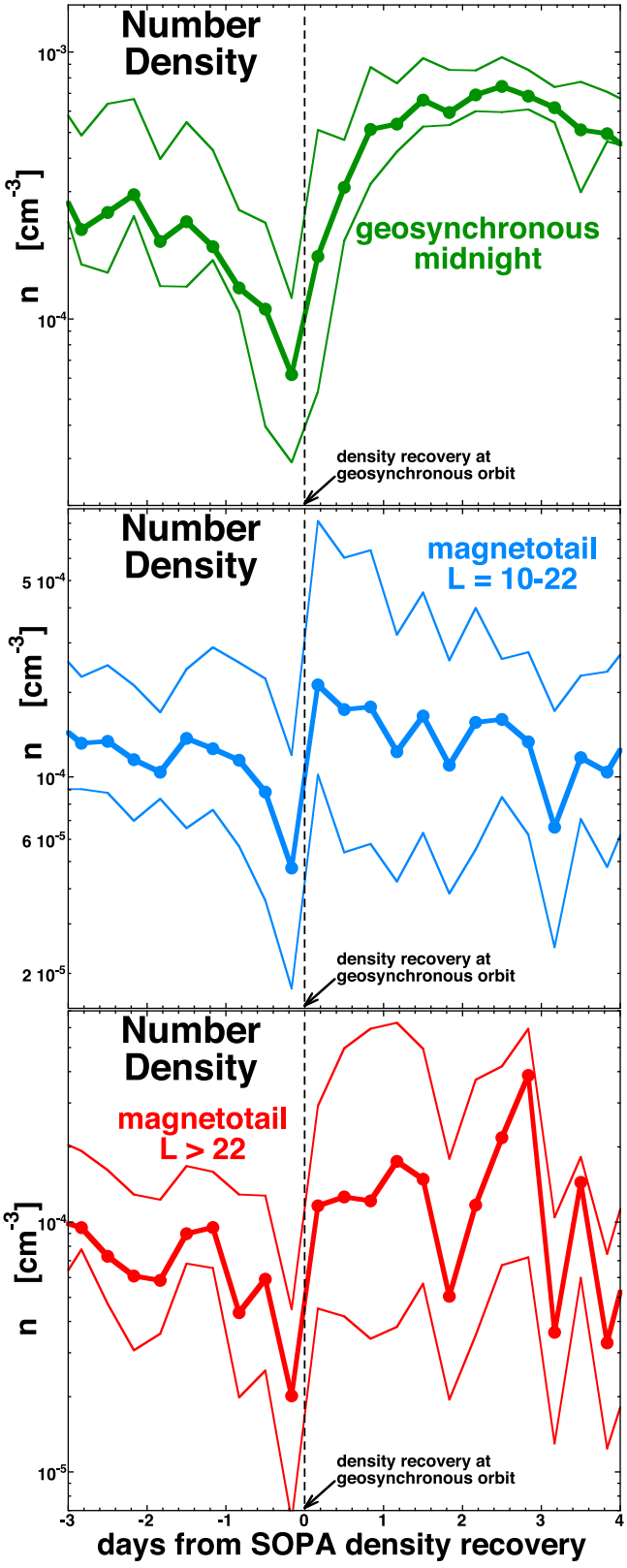

[28] In Figure 7 the superposed median value of the energetic electron differential flux is plotted; the green curve is for 1.3-MeV electrons at geosynchronous-orbit local midnight, the blue curve is for 562-keV electrons in the near-Earth magnetotail, and the red curve is for 562-MeV electrons in the distant magnetotail. Comparing the green and blue curves it is clear that the temporal evolution of the energetic-electron flux is the same in the two regions: a decay before the storm, a mild dropout at about the time t = 0, and a slow rise in intensity in the days of the storm. The red curve in Figure 7 shows those same trends, but with substantial statistical noise.

[29] Figures 3–7 support a picture wherein the outer electron radiation belt at geosynchronous obit goes through four phases associated with high-speed-stream-driven geomagnetic activations: (1) a decay of the number density of the outer electron radiation belt during the calm before the storm, (2) a sudden dropout of the number density of the outer electron radiation belt, (3) a rapid recovery of the number density to a new level, and (4) a heating of the outer electron radiation belt at constant density during the high-speed-stream-driven geomagnetic activity. These are the same four phases as the outer electron radiation belt goes through for high-speed-stream-driven storms [*Denton et al.*, 2010; *Borovsky and Denton*, 2011] (see section 1).

3.2. Reasons for the Radiation Belt Behavior

[30] The behavior of the outer electron radiation belt in three of the four phases has been argued in terms of physical processes acting in the dipolar (middle) magnetosphere. The reasons for the behavior in each of the four phases are described in the following four paragraphs.

[31] In the first phase the number density of the radiation belt decays steadily before the onset of geomagnetic activity. As can be seen in Figure 1b, geomagnetic activity is exceptionally low prior to the geomagnetic activation at time t ~ 0. This is the so-called "calm before the storm." The calm originates for the same reason that the storm originates, a Russell-McPherron effect that drives a storm after a sector reversal will result in a calm before the sector reversal [*Borovsky and Steinberg*, 2006], with the sector reversal occurring a few hours prior to the stream interface upstream of the high-speed wind [*Gosling et al.*, 1978; *Neugebauer*

Figure 4. For the 15 high-speed-stream-driven weak storms of 2006 and 2007, the superposed logarithmic-mean values (central curves with points) and upper and lower quartile values (solid curves without points) are plotted. (top) The outer electron radiation belt at geosynchronous-orbit local midnight, (middle) the near-Earth magnetotail, and (bottom) the more-distant magnetotail. The zero epoch in the horizontal axis is the time of sudden recovery of the number density of the outer electron radiation belt at geosynchronous orbit.

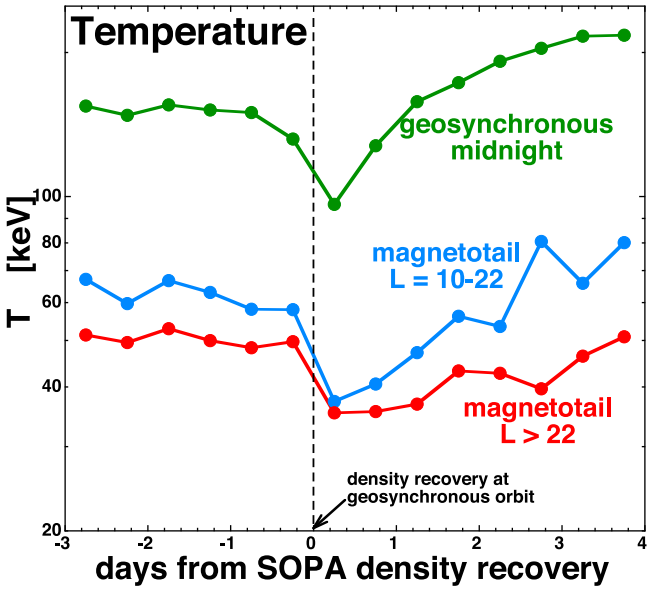

Figure 5. For the 15 high-speed-stream-driven weak storms of 2006 and 2007, the superposed logarithmic average of the energetic-electron temperature is plotted as a function of time. The green curve is for the outer electron radiation belt at geosynchronous-orbit local midnight, the blue curve is for the near-Earth magnetotail, and the red curve is for the more-distant magnetotail. The zero epoch in the horizontal axis is the time of sudden recovery of the number density of the outer electron radiation belt at geosynchronous orbit.

et al., 2004]. During the calm before the storm the outer plasmasphere builds up beyond geosynchronous orbit [*Borovsky et al.*, 1998a; *Borovsky and Steinberg*, 2006; *Borovsky and Denton*, 2009a]. Plasma waves (plasmaspheric whistler mode hiss and electromagnetic ion cyclotron waves) that live in the plasmasphere are believed to pitch angle scatter the radiation-belt electrons into the loss cone [e.g., *Smith et al.*, 1974; *Kelley et al.*, 1975; *Albert*, 2004; *Summers et al.*, 2004; *Shprits and Thorne*, 2004] to produce the pre-storm decay in the number density of the outer electron radiation belt [*Borovsky and Denton*, 2009a].

[32] In the second phase the number density of the outer electron radiation belt drops suddenly prior to the onset of geomagnetic activity, a so-called "radiation-belt dropout" or "density dropout." The dropout is associated with an interval of high-density solar wind caused by the compression of slow solar wind in the corotating interaction region between the masses of slow and fast solar wind. The dropout is commonly attributed to one of three mechanisms: (1) Magnetopause shadowing caused by the compression of the dayside magnetosphere caused by a high solar wind density [*West et al.*, 1972; *Li et al.*, 1997; *Desorgher et al.*, 2000; *Bortnik et al.*, 2006; *Borovsky and Denton*, 2010a] and/or (2) pitch angle scattering into the loss cone [cf. *Longden et al.*, 2008; *Sandanger et al.*, 2009; *Meredith et al.*, 2011] by enhanced pitch angle scattering by plasma waves driven by a superdense plasma sheet caused by leakage of the high-density solar wind into the magnetosphere running into the plasmaspheric drainage plume [*Borovsky et al.*, 1997a, 1998c; *Denton and Borovsky*, 2008; *Borovsky and Denton*, 2009b] which would produce enhanced levels of plasma waves driven by plasma sheet particles (such as electromagnetic ion cyclotron waves [*Cornwall et al.*, 1970; *Fraser and Nguyen*, 2001; *Meredith et al.*, 2003; *Jordanova et al.*, 2006; *Thorne et al.*, 2006]) and/or (3) the Dst effect in which the outer electron radiation belt migrates outward as the ring current diamagnetism inflates the inner magnetosphere pushing magnetic flux outward [*Dessler and Karplus*, 1961; *Kim and Chan*, 1997; *Antonova et al.*, 2009]. Another possible cause of the density dropout is a retreat of the radiation belts to lower L shells during the solar wind compression of the dayside and nightside magnetosphere at about the time of storm onset (J. E. Borovsky and M. H. Denton, Electron-radiation-belt density dropouts and density recoveries, submitted to *Journal of Geophysical Research*, 2011). For the Dst effect moving the outer electron radiation belt outward and for the solar wind compression moving the outer electron radiation belt inward, the behavior in the density-temperature description depends on the radial profile of the radiation belt prior to the magnetic-morphology change and on the radial profile of the morphology change. The number density of the outer electron radiation belt falls off strongly with radius at geosynchronous orbit [*Denton and Cayton*, 2011] so inward compression followed by outward expansion should produce a density decrease followed by a density increase. Simulations to test these predictions for high-speed-stream-driven storms are underway (J. Birn and D. Welling, private communication, 2011).

[33] The third phase, rapid recovery of the radiation-belt number density, is a mystery. The timing of the rapid

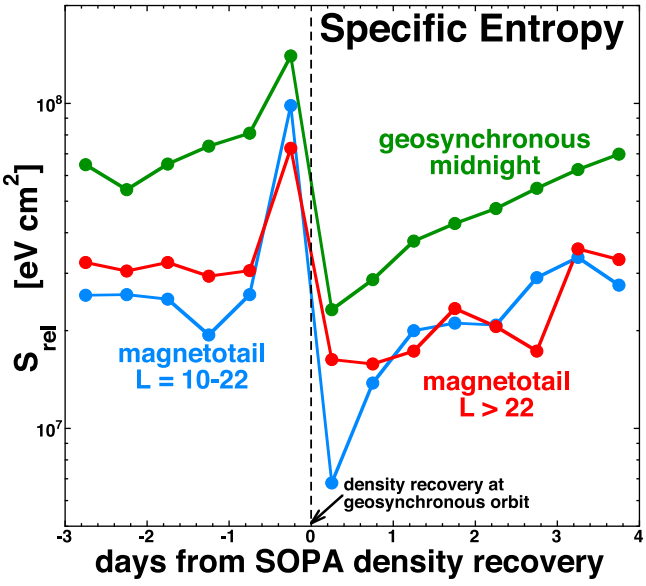

Figure 6. For the 15 high-speed-stream-driven weak storms of 2006 and 2007, the superposed median value of the energetic-electron relativistic specific entropy is plotted as a function of time. The green curve is for the outer electron radiation belt at geosynchronous-orbit local midnight, the blue curve is for the near-Earth magnetotail, and the red curve is for the more-distant magnetotail. The zero epoch in the horizontal axis is the time of sudden recovery of the number density of the outer electron radiation belt at geosynchronous orbit.

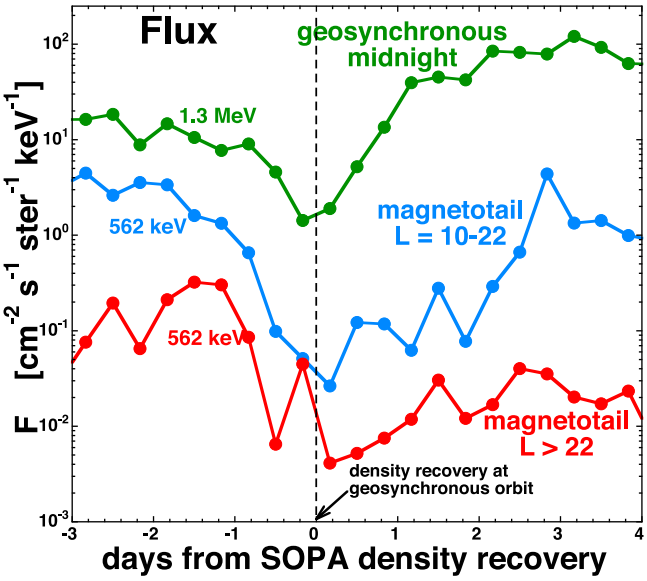

Figure 7. For the 15 high-speed-stream-driven weak storms of 2006 and 2007, the superposed median value of the energetic-electron differential flux is plotted as a function of time. The green curve is for 1.3-MeV electrons in the outer electron radiation belt at geosynchronous-orbit local midnight, the blue curve is for 562-keV electrons in the near-Earth magnetotail, and the red curve is for 562-keV electrons in the more-distant magnetotail. The zero epoch in the horizontal axis is the time of sudden recovery of the number density of the outer electron radiation belt at geosynchronous orbit.

recovery is coincident with a reduction of the enhanced ram pressure of the solar wind. It has been argued that the recovery is associated with the relaxation of the inflated magnetosphere as Dst decreases in magnitude [*Dessler and Karplus*, 1961; *Kim and Chan*, 1997; *Antonova et al.*, 2009], but contrary to this argument the density recovery has been shown to occur prior to Dst relaxation [*Borovsky and Denton*, 2009b, 2010a]. Another possibility is the density recovery is caused by the outward migration of radiation-belt electrons that had retreated to lower L shells when the magnetosphere was compressed by the enhancement of the solar wind ram pressure. Note that it has often been suggested that the source population of the outer electron radiation belt could be the plasma sheet suprathermal electrons injected into the dipolar magnetosphere by substorms [*McDiarmid and Burrows*, 1965; *Borovsky et al.*, 1998a; *Ingraham et al.*, 2001; *Fok et al.*, 2001; *Obara et al.*, 2001; *Varotsou et al.*, 2005]: one could henceforth also suggest that the recovery electrons of the outer electron radiation belt are simply these injected electrons [see also *Antonova et al.*, 2011]. However, contrary to this suggestion, Borovsky and Denton (submitted manuscript, 2011) found that the population of injected electrons and the outer electron radiation belt remain distinct from each other at geosynchronous orbit at the time of density recovery. The cause of the rapid recovery of the outer electron radiation belt, along with the source population for the outer electron radiation belt, can be considered as an outstanding question in magnetospheric physics.

[34] In the fourth phase the outer electron radiation belt heats at constant number density during the high-speed-stream-driven geomagnetic activity. There are three leading-candidate mechanisms for the storm time heating of the outer electron radiation belt: (i) cyclotron-resonant energization of radiation-belt electrons by whistler waves [*Summers and Ma*, 2000; *Albert*, 2004; *Horne et al.*, 2005] or by magnetosonic waves [*Horne et al.*, 2007; *Tao et al.*, 2009], (ii) radial diffusion of radiation-belt electrons driven by random interactions with ULF waves [*Lanzerotti et al.*, 1978; *Perry et al.*, 2005; *Shprits et al.*, 2008a], and (iii) drift-resonant energization of radiation-belt electron by coherent interaction with ULF waves [*Hudson et al.*, 2000; *Elkington et al.*, 2003; *Degeling and Rankin*, 2008]. Recent analysis indicates that a combination of wave acceleration and radial diffusion acts to energize the outer electron radiation belt [*Shprits et al.*, 2008b].

4. Evolution of the Magnetotail Energetic-Electron Population in Comparison With the Outer-Electron-Radiation-Belt Evolution

[35] In Figures 3–6 the superposed logarithmically averaged number density n, superposed logarithmically averaged temperature T, and superposed median specific entropy S_{rel} of the energetic-electron population of the magnetotail are plotted in blue and red where they can be compared with the evolution of those same quantities in the outer electron radiation belt at geosynchronous-orbit midnight. The zero-epoch for the plots is the density recovery of the outer electron radiation belt at geosynchronous orbit for each of the 15 high-speed-stream-driven geomagnetic activations in 2006–2007.

4.1. The Number-Density Behavior of the Energetic-Electron Population

[36] In Figures 3 and 4 the number density of the energetic-electron population of the magnetotail is plotted in blue for $10 \le L \le 22$ (near-Earth tail) and in red for $L > 22$ (distant tail). As can be seen, the general trend of the blue and red curves for the magnetotail energetic-electron population is similar to the general trend of the green curve for geosynchronous-orbit midnight. The number density of the energetic-electron population of the magnetotail is lower than the number density at geosynchronous-orbit midnight, with the number density in the distant tail (red) in general lower than the number density in the near-Earth tail. Note, however, that the statistical noise levels are much higher for the blue and red curves than for the green curve: the blue curve is constructed from 511 measurements, the red curve is constructed from 1006 measurements, and the green curve is constructed from 20,113 measurements. This is an average of 36.5, 71.9, and 1437 measurements per point plotted in the curve for the blue, red, and green curves respectively, where the measurements are not independent (i.e., not from separate events).

[37] In Figure 4 (middle and bottom) the logarithmic mean (with points) and the upper and lower quartiles (without points) are plotted for the number density measurements at $10 \le L \le 22$ (Figure 4, middle) and $L > 22$ (Figure 4, bottom). As can be seen, the trends indicated by the means are reflected by trends in the upper and lower quartiles.

[38] In the days before time t = 0 (where t = 0 is the time of radiation-belt density recovery at geosynchronous orbit) the green curves of Figures 3 and 4 show a steady decay in the number density of the outer electron radiation belt at geosynchronous-orbit midnight: this is the density decay during the calm before the storm. The red and blue curves of Figures 3 and 4 representing the energetic-electron population in the magnetotail also display this decay, but with more statistical noise. This is noted in Table 1.

[39] All curves in Figures 3 and 4 definitely display the density dropout prior to time t = 0: hence the density dropout occurs at geosynchronous-orbit midnight, in the near-Earth magnetotail, and in the distant magnetotail. This is noted in Table 1. To within the 12-h and 8-h accuracies of the plots, all three regions simultaneously experience the dropout.

[40] All curves in Figures 3 and 4 display the rapid recovery from density dropout: hence the density recovery occurs at geosynchronous-orbit midnight, in the near-Earth magnetotail, and in the distant magnetotail. This is noted in Table 1. All recover simultaneously to within the temporal accuracies of the plots. In all three regions of the magnetosphere, the values of number density after recovery are higher than the values of number density before dropout.

[41] After the density recovery the green curves of Figures 3 and 4 show a number density at geosynchronous-orbit midnight that is approximately constant for the 3 days plotted. The red and blue curves of the magnetotail in Figures 3 and 4 show perhaps an approximately constant trend or a slight decay in the number density, with considerable statistical noise.

4.2. The Temperature Behavior of the Energetic-Electron Population

[42] In Figure 5 the temperature T of the energetic-electron population in the magnetotail is plotted in blue for the near-Earth magnetotail ($10 \leq L \leq 22$) and in red for the distant magnetotail ($L > 22$), where it can be compared with the evolution of the temperature of the outer electron radiation belt at geosynchronous-orbit midnight plotted in green. All three curves in Figure 5 show the same basic trends, with the temperature of the energetic-electron population of the magnetotail lower than the temperature at geosynchronous-orbit midnight, and with the temperature in the distant tail (red) lower than the temperature in the near-Earth tail.

[43] As can be seen in Figure 5, before the density dropout the temperature in each of the three regions is approximately constant with time.

[44] The data point in Figure 5 just before t = 0 in each curve represents the temperature during the density dropout. These temperature values can be somewhat dubious owing to the low count rates during the dropouts.

[45] As can be seen in Figure 5, just after density recovery (just after t = 0) the temperature in all three regions is lower than the temperature before density dropout. It has been argued that whatever the source population for the radiation-belt electrons, when the electrons suddenly appear at geosynchronous orbit at recovery they have a temperature of about 100 keV [*Borovsky and Denton*, 2010b]. This may provide a clue as to the seed population of the outer electron radiation belt. In the magnetotail, the temperatures of the electrons at the density recovery are about 40 keV.

[46] As can be seen in Figure 5, in the days of high-speed-stream-driven geomagnetic activity after density recovery, the energetic-electron populations in all three regions experience steady temperature increases with time. This is noted in Table 1. In the t = 1–4 day range in Figure 5, the average daily temperature increase ΔT is 29.6 keV/day for the outer electron radiation belt at geosynchronous-orbit midnight (green curve), 11.6 keV/day for the energetic-electron population in the near-Earth magnetotail (blue curve), and 5.0 keV/day for the energetic-electron population in the distant magnetotail (red curve). The three regions have similar fractional temperature changes $\Delta T/T$ in the t = 1–4 day interval: for the outer electron radiation belt at geosynchronous-orbit midnight the average value of $\Delta T/T$ is 0.17 per day, for the near-Earth magnetotail the average value of $\Delta T/T$ is 0.20 per day, and for the distant magnetotail the average value of $\Delta T/T$ is 0.12 per day.

4.3. The Specific-Entropy Behavior of the Energetic-Electron Population

[47] In Figure 6 the superposed median value of the relativistic specific entropy S_{rel} (as given in expression (1)) for the energetic-electron population in the magnetotail is plotted (red and blue) as a function of time from geosynchronous density recovery for the high-speed-stream-driven activations, in comparison with the median value of the relativistic specific entropy at geosynchronous-orbit midnight (green). As can be seen, the general trend of the three curves is similar.

[48] The most prominent features in all three curves is the large increase in specific entropy during the density dropout (just prior to t = 0) and the large decrease in specific entropy when the density recovers from dropout (going from $t < 0$ to $t > 0$). The specific entropy of the energetic-electron population at all three locations is lower after the density recovers than it was prior to the density dropout.

[49] As can be seen in Figure 6, after density recovery the specific entropy steadily increases during the era of elevated geomagnetic activity. This latter temporal increase in S_{rel} is associated with the steady temporal increase in the temperature T of the energetic-electron populations at constant number density

[50] One difference between the specific entropy evolution in the magnetotail (red and blue curves) and at geosynchronous-orbit midnight (green curve) is the steady increase in the specific entropy during the calm before the storm before the dropout for geosynchronous-orbit midnight that is not seen in the magnetotail curves. This steady increase in the specific entropy during the calm before the storm is associated with the steady decay in the number density at constant temperature during the calm before the storm.

5. Conclusions Drawn From Observations

[51] As seen in section 4, for the high-speed-stream-driven geomagnetic activations the behaviors of the outer electron radiation belt at geosynchronous-orbit local midnight and the energetic-electron population in the magnetotail are largely the same. Both populations show density decays prior to the storms, both show dropouts associated with enhanced solar wind pressure, both show density recoveries to levels higher than the density before dropout, and both show steady heating at approximately constant density during the geomagnetic

activity. The similarity of the behaviors of the two populations, and the simultaneity of the behaviors, argues that the two populations are related. (The similarity of the specific entropies of the two populations also argues that they are related.) It would be difficult to believe the similarity of the behaviors is coincidental.

[52] As noted in section 3.2, some of these behaviors are attributable to physical processes acting in the dipolar magnetosphere associated with the reaction of the magnetosphere to the CIR and the following high-speed stream.

[53] Behavior attributable to physical processes acting on the outer electron radiation belt in the dipole is seen in the energetic-electron population in the magnetotail: hence it will be concluded that the energetic-electron population in the magnetotail mimics the behavior of the outer electron radiation belt in the dipole. This implies that the energetic-electron population of the magnetotail originates from a leakage or evaporation from the outer electron radiation belt.

[54] This is laid out in the following 4 subsections. The conclusions drawn are collected into Table 1.

5.1. The Density-Decay Phase

[55] The outer electron radiation belt at geosynchronous orbit and the energetic-electron population of the magnetotail both exhibit the well-known decay in number density prior to storm onset in Figures 3 and 4.

[56] The pre-storm number density decay of the outer electron radiation belt at geosynchronous orbit can be attributed to scattering into the loss cone by plasmaspheric whistler mode hiss and electromagnetic ion cyclotron waves that live in the plasmasphere [e.g., *Smith et al.*, 1974; *Kelley et al.*, 1975; *Albert*, 2004; *Summers et al.*, 2004; *Shprits and Thorne*, 2004]. The rate of decay correlates with the presence of the plasmasphere [*Borovsky and Denton*, 2009a], which only resides in the dipolar magnetosphere, not in the magnetotail.

[57] The facts (1) that the pre-storm density decay is seen in the dipole at geosynchronous orbit and in the magnetotail and (2) that the cause of the density decay is probably in the dipole indicate that the energetic-electron population of the magnetotail follows the behavior of the outer electron radiation belt in the dipole. This is consistent with the energetic-electron population of the magnetotail being leakage or evaporation from the outer electron radiation belt in the dipole. This conclusion is entered into Table 1.

5.2. The Density-Dropout Phase

[58] The outer electron radiation belt at geosynchronous orbit and the energetic-electron population of the magnetotail both experience the density dropout near the time of storm onset. The dropout is simultaneous to within the 12-h accuracy of the plots in Figure 3.

[59] The number density dropout of the outer electron radiation belt at geosynchronous orbit can be attributed to the compression of the dayside dipolar magnetosphere by the enhanced ram pressure of the high-density solar wind of the CIR. Pressure balance with the high-ram-pressure solar wind at the dayside magnetopause means the magnetic pressure of the magnetosphere at the magnetopause must be high, so the magnetic field strength in the magnetosphere at the magnetopause must be high [*Spreiter et al.*, 1966; *Schield*, 1969]. Energetic electrons in the dipole with equatorial pitch angles near 90° will gradient and curvature drift on paths around the Earth that have equi-magnetic field strength. Energetic electrons in the weakened field on the nightside will not be able to find weak field on the dayside, hence they will drift to the dayside magnetopause and be lost [e.g., *Desorgher et al.*, 2000; *Ukhorskiy et al.*, 2006; *Kim et al.*, 2008]. This process is known as magnetopause shadowing. Aided by radial diffusion [cf. *Shprits et al.*, 2006; *Loto'aniu et al.*, 2010] or by diamagnetic distortion of the magnetosphere [cf. *Kim et al.*, 2010], magnetopause shadowing can deplete much of the outer electron radiation belt. This enhanced-loss argument only works for energetic electrons in the dipolar regions: they are on trapped drift orbits for low solar wind pressure and are lost for high solar wind pressure. The argument does not work for energetic electrons in the magnetotail: they are on drift paths to the flank magnetopause [*Roederer*, 1967; *Fairfield*, 1968] and hence will always be lost from the magnetosphere regardless of the solar wind ram pressure. Hence, the magnetopause-shadowing-caused dropout is a dipole-region phenomenon.

[60] Another suggested mechanism for the radiation-belt density dropout stems from the fact the high-density solar wind of the CIR produces a superdense, extrahot plasma sheet in the magnetosphere [*Borovsky et al.*, 1997a; *Denton and Borovsky*, 2009]. This superdense, extrahot plasma sheet may drive enhanced levels of electromagnetic ion cyclotron or magnetosonic waves in the plasmaspheric drainage plume near local noon [*Borovsky and Denton*, 2009b]. The enhanced plasma waves could lead to rapid pitch angle scattering of radiation-belt electrons into the loss cone, producing the density dropout. The drainage plume cuts across all L shells on the dayside and energetic electrons whose orbit carries them through the dayside magnetosphere are subject to loss as they pass across the plume. This enhanced-loss mechanism works for energetic electrons in the dipolar regions of the magnetosphere since those electrons orbit around the Earth. It does not work for energetic electrons in the magnetotail [*Roederer*, 1967], whose orbits do not carry them across the dayside magnetosphere through the drainage plume. Again, the dropout is a dipole-region phenomenon.

[61] The facts (1) that the dropout is seen in the dipole at geosynchronous orbit and in the magnetotail and (2) that the cause of the dropout is probably in the dipole indicate that the energetic-electron population of the magnetotail follows the behavior of the outer electron radiation belt in the dipole. This is consistent with the energetic-electron population of the magnetotail being leakage or evaporation from the outer electron radiation belt in the dipole. This conclusion is entered into Table 1.

5.3. The Density-Recovery Phase

[62] The outer electron radiation belt at geosynchronous orbit and the energetic-electron population of the magnetotail both experience the rapid density recovery from dropout. The density recovery is simultaneous to within the 12-h accuracy of the plots in Figure 3.

[63] The mechanisms behind the rapid recoveries of the radiation-belt number density from the density-dropout phase are not understood. (Note that the rapid recovery from density dropout comes several hours earlier than the rapid recovery from relativistic-flux dropout: compare Figures 2b and 2c.)

[64] Since the location of the physical process leading to rapid density recovery is not known, the density recovery provides no conclusions as to (a) the behavior of the outer electron radiation belt in the dipole leading the behavior of the energetic-electron population in the magnetotail or (b) the behavior of the energetic-electron population leading the behavior of the outer electron radiation belt. This is noted in Table 1.

5.4. The Heating Phase

[65] The outer electron radiation belt at geosynchronous orbit and the energetic-electron population of the magnetotail both experience the steady heating during the high-speed-stream-driven geomagnetic activity (cf. Figure 5). The relative heating rates $\Delta T/T$ (where ΔT is the change in the temperature over a given time period and T is the temperature) are similar for the outer electron radiation belt at geosynchronous orbit and the energetic-electron population in the magnetotail.

[66] One favored mechanism for the heating of the outer electron radiation belt in the dipolar regions of the magnetosphere is in situ heating of electrons by magnetospheric plasma waves. Theoretical investigations have concluded that this in situ heating could be cyclotron energization by whistler mode chorus waves [*Summers et al.*, 1998, 2004; *Roth et al.*, 1999; *Meredith et al.*, 2001; *Horne et al.*, 2005, 2006], cyclotron energization by magnetosonic waves [*Horne et al.*, 2007; *Tao et al.*, 2009], or drift-resonant energization by ULF waves [*Elkington et al.*, 1999, 2003; *Hudson et al.*, 2000; *Ozeke and Mann*, 2008]. Magnetic pumping by the interaction of ULF plus high-frequency waves may also be important [cf. *Liu et al.*, 1999].

[67] A second favored mechanism for the heating of the outer electron radiation belt is by radial diffusion of radiation-belt electrons by ULF waves [*Lanzerotti et al.*, 1978; *Perry et al.*, 2005; *Shprits et al.*, 2008a]. Numerical simulations of the radial-diffusion heating have concentrated on the dipolar regions of the magnetosphere [e.g., *Bourdarie et al.*, 1996; *Brautigam and Albert*, 2000; *Perry et al.*, 2005; *Jordanova et al.*, 2008; *Lam et al.*, 2009; *Huang et al.*, 2010].

[68] *Shprits et al.* [2008a] argue that a combination of in situ wave energization plus radial diffusion is sufficient to explain the observed heating of the outer electron radiation belt.

[69] The facts (1) that the electron heating (increase in temperature) is seen in the dipole at geosynchronous orbit and in the magnetotail and (2) that the cause of the heating is probably in the dipole indicate that the energetic-electron population of the magnetotail mimics the behavior of the outer electron radiation belt in the dipole. This is consistent with the energetic-electron population of the magnetotail being leakage or evaporation of the outer electron radiation belt in the dipole. This conclusion is entered into Table 1.

6. Summary

[70] The temporal behaviors of the outer electron radiation belt at geosynchronous orbit and of the energetic-electron population in the magnetotail were examined during a set of 15 high-speed-stream-driven geomagnetic activations in the years 2006 and 2007. Four phases of high-speed-stream-driven storms were specifically examined: (1) the number-density decay phase prior to geomagnetic activation, (2) the density-dropout phase at about the time of geomagnetic activation, (3) the density-recovery phase a few hours after dropout, and (4) the heating phase during the extended interval of geomagnetic activity. The findings and conclusions are summarized in Table 1.

[71] In phases 1, 2, 3, and 4 the temporal behavior of the energetic-electron population in the magnetotail is the same as the temporal behavior of the outer electron radiation belt at geosynchronous orbit.

[72] For phases 1, 2, and 4 (density decay, density dropout, and heating) the observations plus our understanding of the physics of the electron radiation belt lead to the conclusion that the energetic-electron population in the magnetotail mimics the outer electron radiation belt in the dipole. This is implies that the energetic-electron population in the magnetotail originates from "leakage" or "outward evaporation" of the outer electron radiation belt.

[73] For phase 3 (density recovery) there is no conclusions that can be drawn from the observations. The temporal behavior of the energetic-electron population of the magnetotail and the outer electron radiation belt are the same, but we have no physical understanding about the cause of this recovery. Note that the phase-3 observations are *consistent with* the energetic-electron population in the magnetotail originating from "leakage" or "outward evaporation" of the outer electron radiation belt.

7. Discussion

[74] An earlier study by *Hones et al.* [1968] based on temporal delays between Injun-4 observations in the dipole and Vela observations in the magnetotail also reached the conclusion that the energetic-electron population of the magnetotail originates from outward transport of radiation-belt electrons from the dipole. That study, however, focused on electrons with energies >45 keV, which includes a mix of both the radiation-belt electrons and some of the higher-energy plasma sheet suprathermal electrons (the "hard" and some of the "soft" electrons in the *Cayton et al.* [1989] and *Denton et al.* [2010] notations).

[75] Previous observations have found that there is a leakage of energetic electrons from the magnetosphere into the magnetosheath and solar wind [*Sarris et al.*, 1987; *Sarafopoulos et al.*, 1999], specifically from the magnetotail. Such observations would be consistent with the conclusion here that there is an outward leakage of outer-radiation-belt electrons from the dipole into the magnetotail.

[76] An earlier study by *Taylor et al.* [2004] examining electron-phase-space gradients between the magnetotail (Cluster spacecraft) and the dipole (SOPA detectors at geosynchronous orbit) found the phase-space density of the energetic electrons to be slightly higher in the magnetotail. These observations were taken as an indication that the plasma sheet energetic electrons could be acting as a source population for the outer electron radiation belt in the dipole. The conclusions of the present study are in contradiction to the *Taylor et al.* [2004] indications. The conclusions of the present study are also in contradiction to theoretical ideas [e.g., *Terasawa and Nishida*, 1976; *Zelenyi et al.*, 1990] that

the source of the energetic-electron population of the magnetotail is in situ energization of electrons in the tail.

[77] The present study finds indications that there is an outward "leakage" or "evaporation" of the outer electron radiation belt from the dipole that is seen in the magnetotail. The mode of outward transport of outer electron radiation belt electrons from the dipole into the magnetotail could be outward radial diffusion [e.g., *Shprits et al.*, 2006, 2008a; *Loto'aniu et al.*, 2010]. In the outer dipolar regions the radial diffusion might be driven by solar wind-driven ULF waves [*Sibeck et al.*, 1989; *Mann et al.*, 1999; *Kepko et al.*, 2002; *Mathie and Mann*, 2000] or internally driven ULF waves [*Hughes et al.*, 1978; *Chen and Hasegawa*, 1988; *Glassmeier et al.*, 1999; *Ozeke and Mann*, 2008] and perhaps that diffusion is enhanced on the nightside by the presence of a cross-tail current sheet encroaching into the dipole. We now suggest that in the magnetotail radial diffusion might be driven by the large-amplitude MHD-turbulence fluctuations of the plasma sheet with its spaghetti magnetic field structure [*Borovsky et al.*, 1997b; *Borovsky and Funsten*, 2003; *Vörös et al.*, 2004; *Weygand et al.*, 2005; *Stepanova et al.*, 2005, 2009; *El-Alaoui et al.*, 2010]: in addition to fluctuations in the E-cross-B drift there are also irregularities in the magnetic field geometries that can lead to diffusion. An investigation into energetic-electron spatial diffusion in the magnetotail's MHD turbulence is called for. *Sergeev et al.* [2008] suggested that radiation-belt electrons might be able to escape the dipolar regions into the magnetotail owing to magnetic field morphology changes associated with near-Earth reconnection.

[78] The evidence for an outward leakage presented in the present study is based on (a) the similarity in temporal behavior of the energetic electrons in the outer electron radiation belt and in the magnetotail and (b) the belief that the temporal behavior is governed by processes occurring in the outer electron radiation belt (i.e., in the dipolar magnetosphere). Note that the SOPA n and T measurements pertain to quasi-isotropic radiation-belt electrons at local midnight and the GPS n and T measurements pertain to the small-equatorial-pitch angle portion of the energetic-electron population in the magnetotail. Acceleration and loss mechanisms may interact differently with isotropic and field-aligned populations.

[79] **Acknowledgments.** The authors wish to thank Evan Noveroske for providing the BDD and CXD data files, Dot Delapp for providing SOPA flux files, and Tom Cayton for providing density-temperature fits for SOPA and GPS. The authors also wish to thank Joachim Birn, Tom Cayton, Steve Morley, Victor Sergeev, and Dan Welling for stimulating conversations. Work at Los Alamos was supported by the NASA Living with a Star TR&T Program, the NSF GEM Program, and the U.S. Department of Energy. Work at Lancaster University was supported by STFC grant ST/G002401/1.

[80] Masaki Fujimoto thanks the reviewers for their assistance in evaluating this paper.

References

Albert, J. M. (2004), Using quasi-linear diffusion to model acceleration and loss from wave-particle interactions, *Space Weather*, *2*, S09S03, doi:10.1029/2004SW000069.

Antonova, E. E., I. P. Kirpichev, M. V. Stepanova, K. G. Orlova, and I. L. Ovchinnikov (2009), Topology of the high latitude magnetosphere during large magnetic storms and the main mechanisms of relativistic electron acceleration, *Adv. Space Res.*, *43*, 628, doi:10.1016/j.asr.2008.09.011.

Antonova, E. E., I. M. Myagkova, M. V. Stapanov, M. O. Riazantseva, I. L. Ovchinnikov, B. B. Mar'in, and M. V. Karavaev (2011), Local particle traps in the high latitude magnetosphere and the acceleration of relativistic electrons, *J. Atmos. Sol. Terr. Phys.*, *73*, 1465, doi:10.1016/j.jastp.2010.11.020.

Baker, D. N., R. L. McPherron, T. E. Cayton, and R. W. Klebesadel (1990), Linear prediction filter analysis of relativistic electron properties at 6.6 R_E, *J. Geophys. Res.*, *95*, 15,133, doi:10.1029/JA095iA09p15133.

Belian, R. D., G. R. Gisler, T. Cayton, and R. Christensen (1992), High-Z energetic particles at geosynchronous orbit during the great solar proton event series of October 1989, *J. Geophys. Res.*, *97*, 16,897, doi:10.1029/92JA01139.

Belian, R. D., T. E. Cayton, R. A. Christiansen, J. C. Ingraham, M. M. Meier, G. D. Reeves, and A. J. Lazarus (1996), Relativistic electrons in the outer-zone: An 11 year cycle; Their relation to the solar wind, in *AIP Proceedings 383 Workshop on the Earth's Trapped Particle Environment*, edited by G. D. Reeves, pp. 13–24, Am. Inst. of Phys., Woodbury, New York.

Bernstein, I. B., E. A. Friemen, M. D. Kruskal, and R. M. Kulsrud (1958), An energy principle for hydromagnetic stability problems, *Proc. R. Soc. London, Ser. A*, *244*, 17, doi:10.1098/rspa.1958.0023.

Birn, J., and K. Schindler (1983), Self-consistent theory of three-dimensional convection in the geomagnetic tail, *J. Geophys. Res.*, *88*, 6969, doi:10.1029/JA088iA09p06969.

Birn, J., M. F. Thomsen, J. E. Borovsky, G. D. Reeves, D. J. McComas, R. D. Belian, and M. Hesse (1998), Substorm electron injections: Geosynchronous observations and test particle simulations, *J. Geophys. Res.*, *103*, 9235, doi:10.1029/97JA02635.

Birn, J., M. F. Thomsen, J. E. Borovsky, G. D. Reeves, and M. Hesse (2000), Particle acceleration in the dynamic magnetotail, *Phys. Plasmas*, *7*, 2149, doi:10.1063/1.874035.

Borovsky, J. E., and T. E. Cayton (2011), Entropy mapping of the outer electron radiation belt between the magnetotail and geosynchronous orbit, *J. Geophys. Res.*, *116*, A06216, doi:10.1029/2011JA016470.

Borovsky, J. E., and M. H. Denton (2006), The differences between CME-driven storms and CIR-driven storms, *J. Geophys. Res.*, *111*, A07S08, doi:10.1029/2005JA011447.

Borovsky, J. E., and M. H. Denton (2009a), Electron loss rates from the outer electron radiation belt caused by the filling of the outer plasmasphere: The calm before the storm, *J. Geophys. Res.*, *114*, A11203, doi:10.1029/2009JA014063.

Borovsky, J. E., and M. H. Denton (2009b), Relativistic-electron dropouts and recovery: A superposed-epoch study of the magnetosphere and the solar wind, *J. Geophys. Res.*, *114*, A02201, doi:10.1029/2008JA013128.

Borovsky, J. E., and M. H. Denton (2010a), The magnetic field at geosynchronous orbit during high-speed-stream-driven storms: Connections to the solar wind, the plasma sheet, and the outer electron radiation belt, *J. Geophys. Res.*, *115*, A08217, doi:10.1029/2009JA015116.

Borovsky, J. E., and M. H. Denton (2010b), On the heating of the outer radiation belt to produce high fluxes of relativistic electrons: Measured heating rates at geosynchronous orbit for high-speed-stream-driven storms, *J. Geophys. Res.*, *115*, A12206, doi:10.1029/2010JA015342.

Borovsky, J. E., and M. H. Denton (2010c), Solar-wind turbulence and shear: A superposed-epoch analysis of corotating interaction regions at 1 AU, *J. Geophys. Res.*, *115*, A10101, doi:10.1029/2009JA014966.

Borovsky, J. E., and M. H. Denton (2011), A survey of the anisotropy of the outer electron radiation belt during high-speed-stream-driven storms, *J. Geophys. Res.*, *116*, A05201, doi:10.1029/2010JA016151.

Borovsky, J. E., and H. O. Funsten (2003), MHD turbulence in the Earth's plasma sheet: Dynamics, dissipation, and driving, *J. Geophys. Res.*, *108*(A7), 1284, doi:10.1029/2002JA009625.

Borovsky, J. E., and J. T. Steinberg (2006), The "calm before the storm" in CIR/magnetosphere interactions: Occurrence statistics, solar-wind statistics, and magnetospheric preconditioning, *J. Geophys. Res.*, *111*, A07S10, doi:10.1029/2005JA011397.

Borovsky, J. E., M. F. Thomsen, and D. J. McComas (1997a), The superdense plasma sheet: Plasmaspheric origin, solar-wind origin, or ionospheric origin? *J. Geophys. Res.*, *102*, 22,089.

Borovsky, J. E., R. C. Elphic, H. O. Funsten, and M. F. Thomsen (1997b), The Earth's plasma sheet as a laboratory for flow turbulence in high-beta MHD, *J. Plasma Phys.*, *57*, 1, doi:10.1017/S0022377896005259.

Borovsky, J. E., M. F. Thomsen, D. J. McComas, T. E. Cayton, and D. J. Knipp (1998a), Magnetospheric dynamics and mass flow during the November 1993 storm, *J. Geophys. Res.*, *103*, 26,373, doi:10.1029/97JA03051.

Borovsky, J. E., M. F. Thomsen, R. C. Elphic, T. E. Cayton, and D. J. McComas (1998b), The transport of plasma-sheet material from the

distant tail to geosynchronous orbit, *J. Geophys. Res.*, *103*, 20,297, doi:10.1029/97JA03144.
Borovsky, J. E., M. F. Thomsen, and R. C. Elphic (1998c), The driving of the plasma sheet by the solar wind, *J. Geophys. Res.*, *103*, 17,617, doi:10.1029/97JA02986.
Bortnik, J., R. M. Thorne, T. P. O'Brien, J. C. Green, R. J. Strangeway, Y. Y. Shprits, and D. N. Baker (2006), Observation of two distinct, rapid loss mechanisms during the 20 November 2003 radiation belt dropout event, *J. Geophys. Res.*, *111*, A12216, doi:10.1029/2006JA011802.
Bourdarie, S., D. Boscher, T. Beutier, J.-A. Sauvaud, and M. Blanc (1996), Magnetic storm modeling in the Earth's electron belt by the Salammbo code, *J. Geophys. Res.*, *101*, 27,171, doi:10.1029/96JA02284.
Brautigam, D. H., and J. M. Albert (2000), Radial diffusion analysis of outer radiation belt electrons during the October 9, 1990, magnetic storm, *J. Geophys. Res.*, *105*, 291, doi:10.1029/1999JA900344.
Cayton, T. E., and R. D. Belian (2007), Numerical modeling of the synchronous orbit particle analyzer, *Rep. LA-14335*, Los Alamos Natl. Lab., Los Alamos, N. M., June.
Cayton, T. E., R. D. Belian, S. P. Gary, T. A. Fritz, and D. N. Baker (1989), Energetic electron components at geosynchronous orbit, *Geophys. Res. Lett.*, *16*, 147, doi:10.1029/GL016i002p00147.
Cayton, T. E., D. M. Drake, K. M. Spencer, M. Herrin, T. J. Wehenr, and R. C. Reedy (1998), Description of the BDD-IIR: Electron and proton sensors on the GPS, *Tech. Rep. LA-UR-98-1162*, Los Alamos Natl. Lab., Los Alamos, N. M.
Cayton, T. E., Y. Chen, R. H. W. Friedel, and R. M. Kippen (2010), Analysis of electron and proton environmental data for medium-Earth orbit (2000–present), *Tech. Rep. LA-UR-10-4234*, Los Alamos Natl. Lab., Los Alamos, N. M.
Chen, L., and A. Hasegawa (1988), On magnetospheric hydromagnetic waves excited by energetic ring-current particles, *J. Geophys. Res.*, *93*, 8763, doi:10.1029/JA093iA08p08763.
Cornwall, J. M., F. V. Coroniti, and R. M. Thorne (1970), Turbulent loss of ring current protons, *J. Geophys. Res.*, *75*, 4699, doi:10.1029/JA075i025p04699.
Degeling, A. W., and R. Rankin (2008), Resonant drift echoes in electron phase space density produced by dayside Pc5 waves following a geomagnetic storm, *J. Geophys. Res.*, *113*, A10220, doi:10.1029/2008JA013254.
Denton, M. H., and J. E. Borovsky (2008), Superposed epoch analysis of high-speed-stream effects at geosynchronous orbit: Hot plasma, cold plasma, and the solar wind, *J. Geophys. Res.*, *113*, A07216, doi:10.1029/2007JA012998.
Denton, M. H., and J. E. Borovsky (2009), The superdense plasma sheet in the magnetosphere during high-speed-steam-driven storms: Plasma transport timescales, *J. Atmos. Sol. Terr. Phys.*, *71*, 1045, doi:10.1016/j.jastp.2008.04.023.
Denton, M. H., and T. E. Cayton (2011), Density and temperature of energetic electrons in the Earth's magnetotail derived from high-latitude GPS observations during the declining phase of the solar cycle, *Ann. Geophys.*, *29*, 1755, doi:10.5194/angeo-29-1755-2011.
Denton, M. H., J. E. Borovsky, R. B. Horne, R. L. McPherron, S. K. Morley, and B. T. Tsurutani (2008), High-speed solar wind streams: A call for key research, *Eos Trans. AGU*, *89*(7), 62, doi:10.1029/2008EO070002.
Denton, M. H., J. E. Borovsky, R. B. Horne, R. L. McPherron, S. K. Morley, and B. T. Tsurutani (2009), Introduction to special issue on high speed solar wind streams and geospace interactions (HSS-GI), *J. Atmos. Sol. Terr. Phys.*, *71*, 1011, doi:10.1016/j.jastp.2008.09.019.
Denton, M. H., J. E. Borovsky, and T. E. Cayton (2010), A density-temperature description of the outer electron radiation belt during geomagnetic storms, *J. Geophys. Res.*, *115*, A01208, doi:10.1029/2009JA014183.
Desorgher, L., E. Fluckiger, P. Buhler, and A. Zehnder (2000), Modelling of the outer electron belt flux dropout and losses during magnetic storm main phase, *Adv. Space Res.*, *26*, 167, doi:10.1016/S0273-1177(99)01044-3.
Dessler, A. J., and R. Karplus (1960), Some properties of the Van Allen radiation, *Phys. Rev. Lett.*, *4*, 271, doi:10.1103/PhysRevLett.4.271.
Dessler, A. J., and R. Karplus (1961), Some effects of diamagnetic ring currents on Van Allen radiation, *J. Geophys. Res.*, *66*, 2289, doi:10.1029/JZ066i008p02289.
Distel, J. R., et al. (1999), The combined X-ray dosimeter (CXD) on GPS block IIR satellites, *Tech. Rep. LA-UR-99-2280*, Los Alamos Natl. Lab., Los Alamos, N. M.
El-Alaoui, M., M. Ashour-Abdalla, R. L. Richard, M. L. Goldstein, J. M. Weygand, and R. J. Walker (2010), Global magnetohydrodynamic simulation of reconnection and turbulence in the plasma sheet, *J. Geophys. Res.*, *115*, A12236, doi:10.1029/2010JA015653.
Elkington, S. R., M. K. Hudson, and A. A. Chan (1999), Acceleration of relativistic electrons via drift-resonant interaction with toroidal-mode PC-5 ULF oscillations, *Geophys. Res. Lett.*, *26*, 3273, doi:10.1029/1999GL003659.
Elkington, S. R., M. K. Hudson, and A. A. Chan (2003), Resonant acceleration and diffusion of outer zone electrons in an asymmetric geomagnetic field, *J. Geophys. Res.*, *108*(A3), 1116, doi:10.1029/2001JA009202.
Fairfield, D. H. (1968), Average magnetic field configuration of the outer magnetosphere, *J. Geophys. Res.*, *73*, 7329, doi:10.1029/JA073i023p07329.
Fok, M.-C., T. E. Moore, and W. N. Spjeldvik (2001), Rapid enhancement of radiation belt electron fluxes due to substorm depolarization of the geomagnetic field, *J. Geophys. Res.*, *106*, 3873, doi:10.1029/2000JA000150.
Fraser, B. J., and T. S. Nguyen (2001), Is the plasmapause a preferred source region of electromagnetic ion cyclotron waves in the magnetosphere? *J. Atmos. Sol. Terr. Phys.*, *63*, 1225, doi:10.1016/S1364-6826(00)00225-X.
Friedel, R. H. W., G. D. Reeves, and T. Obara (2002), Relativistic electron dynamics in the inner magnetosphere—A review, *J. Atmos. Sol. Terr. Phys.*, *64*, 265, doi:10.1016/S1364-6826(01)00088-8.
Fritz, T. A., M. Alothman, J. Bhattacharjya, D. L. Matthews, and J. Chen (2003), Butterfly pitch-angle distributions observed by ISEE-1, *Planet. Space Sci.*, *51*, 205, doi:10.1016/S0032-0633(02)00202-7.
Glassmeier, K.-H., S. Buchert, U. Motschmann, A. Korth, and A. Pedersen (1999), Concerning the generation of geomagnetic giant pulsations by drift-bounce resonance ring current instabilities, *Ann. Geophys.*, *17*, 338, doi:10.1007/s00585-999-0338-4.
Goertz, C. K., and W. Baumjohann (1991), On the thermodynamics of the plasma sheet, *J. Geophys. Res.*, *96*, 20,991, doi:10.1029/91JA02128.
Gosling, J. T., J. R. Asbridge, S. J. Bame, and W. C. Feldman (1978), Solar wind stream interfaces, *J. Geophys. Res.*, *83*, 1401, doi:10.1029/JA083iA04p01401.
Graham, R. (1994), Killer electrons on rise: LANL, *Albuquerque J.*, B8.
Hess, W. N., and J. A. Poirier (1962), Energy spectrum of electrons in the outer radiation belt, *J. Geophys. Res.*, *67*, 1699, doi:10.1029/JZ067i005p01699.
Hilton, H. H. (1971), L parameter, a new approximation, *J. Geophys. Res.*, *76*, 6952, doi:10.1029/JA076i028p06952.
Hones, E. W. (1963), Motions of charged particles trapped in the Earth's magnetosphere, *J. Geophys. Res.*, *68*, 1209, doi:10.1029/JZ068i005p01209.
Hones, E. W., S. Singer, and C. S. R. Rao (1968), Simultaneous observations of electrons (E > 45 keV) at 2000-kilometer altitude and at 100,000 kilometers in the magnetotail, *J. Geophys. Res.*, *73*, 7339, doi:10.1029/JA073i023p07339.
Horne, R. B., et al. (2005), Timescale for radiation belt electron acceleration by whistler mode chorus waves, *J. Geophys. Res.*, *110*, A03225, doi:10.1029/2004JA010811.
Horne, R. B., N. P. Meredith, S. A. Glauert, A. Varotsou, D. Boscher, R. M. Thorne, Y. Y. Shprits, and R. R. Anderson (2006), Mechanisms for the acceleration of radiation belt electrons, in *Recurrent Magnetic Storms*, *Geophys. Monogr. Ser.*, vol. 167, pp. 151–173, AGU, Washington, D. C.
Horne, R. B., R. M. Thorne, S. A. Glauert, N. P. Meredith, D. Pokhotelov, and O. Santolik (2007), Electron acceleration in the Van Allen radiation belts by fast magnetosonic waves, *Geophys. Res. Lett.*, *34*, L17107, doi:10.1029/2007GL030267.
Huang, C.-L., H. E. Spence, M. K. Hudson, and S. R. Elkington (2010), Modeling radiation belt radial diffusion in ULF wave fields: 2. Estimating rates of radial diffusion using combined MHD and particle codes, *J. Geophys. Res.*, *115*, A06216, doi:10.1029/2009JA014918.
Hudson, M. K., S. R. Elkington, J. G. Lyon, and C. C. Goodrich (2000), Increase in relativistic electron flux in the inner magnetosphere: ULF wave mode structure, *Adv. Space Res.*, *25*, 2327, doi:10.1016/S0273-1177(99)00518-9.
Hudson, M. K., B. T. Kress, H. R. Mueller, J. A. Zastrow, and J. B. Blake (2008), Relationship of the Van Allen radiation belts to solar wind drivers, *J. Atmos. Sol. Terr. Phys.*, *70*, 708, doi:10.1016/j.jastp.2007.11.003.
Hughes, W. J., D. J. Southwood, B. Mauk, R. L. McPherron, and J. N. Barfield (1978), Alfven waves generated by an inverted plasma energy distribution, *Nature*, *275*, 43, doi:10.1038/275043a0.
Ingraham, J. C., T. E. Cayton, R. D. Belian, R. A. Christensen, R. H. W. Friedel, M. M. Meier, G. D. Reeves, and M. Tuszewski (2001), Substorm injection of relativistic electrons to geosynchronous orbit during the great magnetic storm of March 24, 1991, *J. Geophys. Res.*, *106*, 25,759, doi:10.1029/2000JA000458.

Jordanova, V. K., Y. S. Miyoshi, S. Zaharia, M. F. Thomsen, G. D. Reeves, D. S. Evans, C. G. Mouikis, and J. F. Fennell (2006), Kinetic simulations of ring current evolution during the Geospace Environment Modeling challenge events, *J. Geophys. Res.*, *111*, A11S10, doi:10.1029/2006JA011644.

Jordanova, V. K., J. Albert, and Y. Miyoshi (2008), Relativistic electron precipitation by EMIC waves from self-consistent global simulations, *J. Geophys. Res.*, *113*, A00A10, doi:10.1029/2008JA013239.

Kavanagh, A. J., and M. H. Denton (2007), High-speed solar-wind streams and geospace interactions, *Astron. Geophys.*, *48*, 6.24.

Kaye, S. M., C. S. Lin, G. K. Parks, and J. R. Winckler (1978), Adiabatic modulation of equatorial pitch angle anisotropy, *J. Geophys. Res.*, *83*, 2675, doi:10.1029/JA083iA06p02675.

Kelley, M. C., B. T. Tsurutani, and F. S. Mozer (1975), Properties of ELF electromagnetic waves in and above the Earth's ionosphere deduced from plasma wave experiments on the OVI-17 and OGO 6 satellites, *J. Geophys. Res.*, *80*, 4603, doi:10.1029/JA080i034p04603.

Kepko, L., H. E. Spence, and H. J. Singer (2002), ULF waves in the solar wind as direct drivers of magnetospheric pulsations, *Geophys. Res. Lett.*, *29*(8), 1197, doi:10.1029/2001GL014405.

Kim, H.-J., and A. A. Chan (1997), Fully adiabatic changes in storm time relativistic electron fluxes, *J. Geophys. Res.*, *102*, 22,107, doi:10.1029/97JA01814.

Kim, K. C., D.-Y. Lee, H.-J. Kim, L. R. Lyons, E. S. Lee, M. K. Ozturk, and C. R. Choi (2008), Numerical calculations of relativistic electron drift loss effect, *J. Geophys. Res.*, *113*, A09212, doi:10.1029/2007JA013011.

Kim, K. C., D.-Y. Lee, H.-J. Kim, E. S. Lee, and C. R. Choi (2010), Numerical estimates of drift loss and Dst effect for outer radiation belt relativistic electrons with arbitrary pitch angle, *J. Geophys. Res.*, *115*, A03208, doi:10.1029/2009JA014523.

Lam, M. M., R. B. Horne, N. P. Meredith, and S. A. Glauert (2009), Radiation belt electron flux variability during three CIR-driven geomagnetic storms, *J. Atmos. Sol. Terr. Phys.*, *71*, 1145, doi:10.1016/j.jastp.2008.06.007.

Lanzerotti, L. J., D. C. Webb, and C. W. Arthur (1978), Geomagnetic field fluctuations at synchronous orbit: 2. Radial diffusion, *J. Geophys. Res.*, *83*, 3866, doi:10.1029/JA083iA08p03866.

Lezniak, T. W., R. L. Arnoldy, G. K. Parks, and J. R. Winkler (1968), Measurements and intensity of energetic electrons at the equator at 6.6 RE, *Radio Sci.*, *3*, 710.

Li, X., D. N. Baker, M. Temerin, T. E. Cayton, E. G. D. Reeves, R. A. Christensen, J. B. Blake, M. D. Looper, R. Nakamura, and S. G. Kanekal (1997), Multispacecraft observations of the outer zone electron variation during the November 3–4, 1993, magnetic storm, *J. Geophys. Res.*, *102*, 14,123, doi:10.1029/97JA01101.

Liu, W. W., G. Rostoker, and D. N. Baker (1999), Internal acceleration of relativistic electrons by large-amplitude ULF pulsations, *J. Geophys. Res.*, *104*, 17,391, doi:10.1029/1999JA900168.

Longden, N., M. H. Denton, and F. Honary (2008), Particle precipitation during ICME-driven and CIR-driven geomagnetic storms, *J. Geophys. Res.*, *113*, A06205, doi:10.1029/2007JA012752.

Loto'aniu, T. M., H. J. Singer, C. L. Waters, V. Angelopoulos, I. R. Mann, S. R. Elkington, and J. W. Bonnell (2010), Relativistic electron loss due to ultralow frequency waves and enhanced outward radial diffusion, *J. Geophys. Res.*, *115*, A12245, doi:10.1029/2010JA015755.

Mann, I. R., A. N. Wright, K. J. Mills, and V. M. Nakariakov (1999), Excitation of magnetospheric waveguide modes by magnetosheath flows, *J. Geophys. Res.*, *104*, 333, doi:10.1029/1998JA900026.

Mathie, R. A., and I. R. Mann (2000), Observations of Pc5 field line resonance azimuthal phase speeds: A diagnostic of their excitation mechanism, *J. Geophys. Res.*, *105*, 10,713, doi:10.1029/1999JA000174.

McDiarmid, I. B., and J. R. Burrows (1965), On an electron source for the outer Van Allen radiation zone, *Can. J. Phys.*, *43*, 1161, doi:10.1139/p65-113.

McIlwain, C. E. (1961), Coordinates for mapping the distribution of magnetically trapped particles, *J. Geophys. Res.*, *66*, 3681, doi:10.1029/JZ066i011p03681.

McPherron, R. L., D. N. Baker, and N. U. Crooker (2009), Role of the Russell-McPherron effect in the acceleration of relativistic electrons, *J. Atmos. Sol. Terr. Phys.*, *71*, 1032, doi:10.1016/j.jastp.2008.11.002.

Meng, C.-I., A. T. Y. Lui, S. M. Krimigis, S. Ismail, and D. J. Williams (1981), Spatial distribution of energetic particles in the distant magnetotail, *J. Geophys. Res.*, *86*, 5682, doi:10.1029/JA086iA07p05682.

Meredith, N. P., R. B. Horne, and R. R. Anderson (2001), Substorm dependence of chorus amplitudes: Implications for the acceleration of electrons to relativistic energies, *J. Geophys. Res.*, *106*, 13,165, doi:10.1029/2000JA900156.

Meredith, N. P., R. M. Thorne, R. B. Horne, D. Summers, B. J. Fraser, and R. R. Anderson (2003), Statistical analysis of relativistic electron energies for cyclotron resonance with EMIC waves observed on CRRES, *J. Geophys. Res.*, *108*(A6), 1250, doi:10.1029/2002JA009700.

Meredith, N. P., R. B. Horne, M. M. Lam, M. H. Denton, J. E. Borovsky, and J. C. Green (2011), Energetic electron precipitation during high-speed solar wind stream driven storms, *J. Geophys. Res.*, *116*, A05223, doi:10.1029/2010JA016293.

Miyoshi, Y., and R. Kataoka (2011), Solar cycle variations of outer radiation belt and its relationship to solar wind structure dependencies, *J. Atmos. Sol. Terr. Phys.*, *73*, 77, doi:10.1016/j.jastp.2010.09.031.

Montgomery, M. D., S. Singer, J. P. Conner, and E. E. Stogsdill (1965), Spatial distribution, energy spectra, and time variations of energetic electrons (E > 50 keV) at 17.7 Earth radii, *Phys. Rev. Lett.*, *14*, 209, doi:10.1103/PhysRevLett.14.209.

Morley, S. K. (2010), Introduction geospace effects of high-speed solar wind streams, *Proc. R. Soc. A*, *466*, 3275, doi:10.1098/rspa.2010.0371.

Nagai, T. (1988), "Space weather forecast": Prediction of relativistic electron intensity at synchronous orbit, *Geophys. Res. Lett.*, *15*, 425, doi:10.1029/GL015i005p00425.

Neugebauer, M., P. C. Liewer, B. E. Goldstein, X. Zhou, and J. T. Steinberg (2004), Solar wind stream interaction regions without sector boundaries, *J. Geophys. Res.*, *109*, A10102, doi:10.1029/2004JA010456.

Obara, T., Y. Miyoshi, and A. Morioka (2001), Large enhancement of the outer belt electrons during magnetic storms, *Earth Planets Space*, *53*, 1163.

Ozeke, L. G., and I. R. Mann (2008), Energization of radiation belt electrons by ring current ion driven ULF waves, *J. Geophys. Res.*, *113*, A02201, doi:10.1029/2007JA012468.

Peredo, M., D. P. Stern, and N. A. Tsyganenko (1993), Are existing magnetospheric models excessively stretched? *J. Geophys. Res.*, *98*, 15,343, doi:10.1029/93JA01150.

Perry, K. L., M. K. Hudson, and S. R. Elkington (2005), Incorporating spectral characteristics of Pc5 waves into three-dimensional radiation belt modeling and the diffusion of relativistic electrons, *J. Geophys. Res.*, *110*, A03215, doi:10.1029/2004JA010760.

Pfitzer, K. A., T. W. Lezniak, and J. R. Winckler (1969), Experimental verification of drift-shell splitting in the distorted magnetosphere, *J. Geophys. Res.*, *74*, 4687, doi:10.1029/JA074i019p04687.

Pierrard, V., and J. Lemaire (1996), Fitting the AE-8 energy spectra with two Maxwellian functions, *Radiat. Meas.*, *26*, 333–337, doi:10.1016/1350-4487(96)00057-1.

Pulkkinen, T. I., and N. A. Tsyganenko (1996), Testing the accuracy of magnetospheric model field line mapping, *J. Geophys. Res.*, *101*, 27,431, doi:10.1029/96JA02489.

Retzler, J., and J. A. Simpson (1969), Relativistic electrons confined within the neutral sheet of the geomagnetic tail, *J. Geophys. Res.*, *74*, 2149, doi:10.1029/JA074i009p02149.

Richter, A. K., and A. H. Luttrell (1986), Superposed epoch analysis of corotating interaction regions at 0.3 and 1.0 AU: A comparative study, *J. Geophys. Res.*, *91*, 5873, doi:10.1029/JA091iA05p05873.

Roederer, J. G. (1967), On the adiabatic motion of energetic particles in a model magnetosphere, *J. Geophys. Res.*, *72*, 981, doi:10.1029/JZ072i003p00981.

Roth, I., M. Temerin, and M. K. Hudson (1999), Resonant enhancement of relativistic electron fluxes during geomagnetically active periods, *Ann. Geophys.*, *17*, 631, doi:10.1007/s00585-999-0631-2.

Sandanger, M. I., F. Soraas, M. Sorbo, K. Aarsnes, K. Oksavik, and D. S. Evans (2009), Relativistic electron loss related to EMIC waves during CIR and CME storms, *J. Atmos. Sol. Terr. Phys.*, *71*, 1126, doi:10.1016/j.jastp.2008.07.006.

Sarafopoulos, D. V., M. A. Athanasiu, E. T. Sarris, T. Yamamoto, and S. Kokubun (1999), Properties and origin of energetic particles at the duskside of the Earth's magnetosheath throughout a great storm, *Ann. Geophys.*, *17*, 1121.

Sarris, E. T., S. M. Krimigis, and T. P. Armstrong (1976), Observations of magnetospheric bursts of high-energy protons and electrons at ~35 R_E with Imp 7, *J. Geophys. Res.*, *81*, 2341, doi:10.1029/JA081i013p02341.

Sarris, E. T., G. C. Anagnostopoulos, and S. M. Krimigis (1987), Simultaneous measurements of energetic ion (E ≥ 50 keV) and electron (E ≥ 220 keV) activity upstream of Earth's bow shock and inside the plasma sheet: Magnetospheric source for the November 3 and December 3, 1977 upstream events, *J. Geophys. Res.*, *92*, 12,083, doi:10.1029/JA092iA11p12083.

Schield, M. A. (1969), Pressure balance between solar wind and magnetosphere, *J. Geophys. Res.*, *74*, 1275, doi:10.1029/JA074i005p01275.

Selesnick, R. S., and J. B. Blake (2002), Relativistic electron drift shell splitting, *J. Geophys. Res.*, *107*(A9), 1265, doi:10.1029/2001JA009179.

Sergeev, V., et al. (2008), Study of near-Earth reconnection events with Cluster and Double Star, *J. Geophys. Res.*, *113*, A07S36, doi:10.1029/2007JA012902.

Shprits, Y. Y., and R. M. Thorne (2004), Time dependent radial diffusion modeling of relativistic electrons with realistic loss rates, *Geophys. Res. Lett.*, *31*, L08805, doi:10.1029/2004GL019591.

Shprits, Y. Y., R. M. Thorne, R. Friedel, G. D. Reeves, J. Fennell, D. N. Baker, and S. G. Kanekal (2006), Outward radial diffusion driven by losses at magnetopause, *J. Geophys. Res.*, *111*, A11214, doi:10.1029/2006JA011657.

Shprits, Y. Y., S. R. Elkington, N. P. Meredith, and D. A. Subbotin (2008a), Review of modeling of losses and sources of relativistic electrons in the outer radiation belt I: Radial transport, *J. Atmos. Sol. Terr. Phys.*, *70*, 1679.

Shprits, Y. Y., D. A. Subbotin, N. P. Meredith, and S. R. Elkington (2008b), Review of modeling of losses and sources of relativistic electrons in the outer radiation belt II: Local acceleration and losses, *J. Atmos. Sol. Terr. Phys.*, *70*, 1694.

Sibeck, D. G., W. Baumjohann, and R. E. Lopez (1989), Solar wind dynamic pressure variations and transient magnetospheric signatures, *Geophys. Res. Lett.*, *16*, 13, doi:10.1029/GL016i001p00013.

Smith, E. J., A. M. A. Frandsen, B. T. Tsurutani, R. M. Thorne, and K. W. Chan (1974), Plasmaspheric hiss intensity variations during magnetic storms, *J. Geophys. Res.*, *79*, 2507, doi:10.1029/JA079i016p02507.

Spreiter, J. R., A. L. Summers, and A. Y. Alksne (1966), Hydromagnetic flow around the magnetosphere, *Planet. Space Sci.*, *14*, 223, doi:10.1016/0032-0633(66)90124-3.

Stepanova, M., T. Vucina-Parga, E. Antonova, I. Ovchinnikov, and Y. Yermolaev (2005), Variation of the plasma turbulence in the central plasma sheet during substorm phases observed by the Interball/Tail satellite, *J. Atmos. Sol. Terr. Phys.*, *67*, 1815, doi:10.1016/j.jastp.2005.01.013.

Stepanova, M., E. Antonova, and J. M. Bosqued (2008), Study of plasma pressure distribution in the inner magnetosphere using the low altitude satellite data and its relevance for magnetospheric dynamics, *J. Phys.*, *134*, 012043, doi:10.1088/1742-6596/134/1/012043.

Stepanova, M. E. E., et al. (2009), Spatial variation of eddy-diffusion coefficients in the turbulent plasma sheet during substorms, *Ann. Geophys.*, *27*, 1407, doi:10.5194/angeo-27-1407-2009.

Summers, D., and C. Y. Ma (2000), A model for generating relativistic electrons in the Earth's inner magnetosphere based on gyroresonant wave-particle interactions, *J. Geophys. Res.*, *105*, 2625, doi:10.1029/1999JA900444.

Summers, D., R. M. Thorne, and F. Xiao (1998), Relativistic theory of wave-particle resonant diffusion with application to electron acceleration in the magnetosphere, *J. Geophys. Res.*, *103*, 20,487, doi:10.1029/98JA01740.

Summers, D., C. Ma, and T. Mukai (2004), Competition between acceleration and loss mechanisms of relativistic electrons during geomagnetic storms, *J. Geophys. Res.*, *109*, A04221, doi:10.1029/2004JA010437.

Tao, X., J. M. Albert, and A. A. Chan (2009), Numerical modeling of multidimensional diffusion in the radiation belts using layer methods, *J. Geophys. Res.*, *114*, A02215, doi:10.1029/2008JA013826.

Taylor, M. G. G. T., R. H. W. Friedel, G. D. Reeves, M. W. Dunlop, T. A. Fritz, P. W. Daly, and A. Balogh (2004), Multisatellite measurements of electron phase space density gradients in the Earth's inner and outer magnetosphere, *J. Geophys. Res.*, *109*, A05220, doi:10.1029/2003JA010294.

Terasawa, T., and A. Nishida (1976), Simultaneous observations of relativistic electron bursts and neutral-line signatures in the magnetotail, Planet. *Space Sci.*, *24*, 855, doi:10.1016/0032-0633(76)90076-3.

Thorne, R. M., R. B. Horne, V. K. Jordanova, J. Bortnik, and S. Glauert (2006), Interaction of EMIC waves with thermal plasma and radiation belt particles, in *Magnetospheric ULF Waves*, edited by K. Takahashi et al., pp. 213–223, AGU, Washington, D. C., doi:10.1029/169GM14.

Tsurutani, B., R. McPherron, W. Gonzalez, G. Lu, J. H. A. Sobral, and N. Gopalswamy (Eds.) (2006), *Recurrent Magnetic Storms*, AGU, Washington, D. C.

Tsyganenko, N. A. (1989), A magnetospheric magnetic field model with a warped tail current sheet, *Planet. Space Sci.*, *37*, 5, doi:10.1016/0032-0633(89)90066-4.

Tuszewski, M. G., T. E. Cayton, and J. C. Ingraham (2002), A new numerical technique to design satellite energetic electron detectors, *Nucl. Instrum. Methods Phys. Res., Sect. A*, *482*, 653, doi:10.1016/S0168-9002(01)01735-1.

Ukhorskiy, A. Y., B. J. Anderson, P. C. Brandt, and N. A. Tsyganenko (2006), Storm time evolution of the outer radiation belt: Transport and losses, *J. Geophys. Res.*, *111*, A11S03, doi:10.1029/2006JA011690.

Varotsou, A., D. Balcher, S. Bourdarie, R. B. Horne, S. A. Glauert, and N. P. Meredith (2005), Simulation of the outer radiation belt electrons near geosynchronous orbit including both radial diffusion and resonant interaction with whistler-mode chorus waves, *Geophys. Res. Lett.*, *32*, L19106, doi:10.1029/2005GL023282.

Vernov, S. N., A. E. Chudakov, E. V. Gorchakov, J. L. Logachev, and P. V. Vakulov (1959), Study of the cosmic-ray soft component by the 3rd Soviet Earth satellite, *Planet. Space Sci.*, *1*, 86, doi:10.1016/0032-0633(59)90002-9.

Vernov, S. N., E. V. Gorchakov, S. N. Kuznetsov, Y. I. Logachev, E. N. Sosnovets, and V. G. Stolpovsky (1969), Particle fluxes in the outer geomagnetic field, *Rev. Geophys.*, *7*, 257, doi:10.1029/RG007i001p00257.

Vörös, Z., et al. (2004), Magnetic turbulence in the plasma sheet, *J. Geophys. Res.*, *109*, A11215, doi:10.1029/2004JA010404.

West, H. I., R. M. Buck, and J. R. Walton (1972), Shadowing of electron azimuthal-drift motions near the noon magnetopause, *Nature Phys. Sci.*, *240*, 6.

Weygand, J. M., et al. (2005), Plasma sheet turbulence observed by Cluster II, *J. Geophys. Res.*, *110*, A01205, doi:10.1029/2004JA010581.

Wing, S., and P. T. Newell (1998), Central plasma sheet ion properties as inferred from ionospheric observations, *J. Geophys. Res.*, *103*, 6785, doi:10.1029/97JA02994.

Zelenyi, L. M., J. G. Lominadze, and A. L. Taktakishvili (1990), Generation of the energetic proton and electron bursts in planetary magnetotails, *J. Geophys. Res.*, *95*, 3883, doi:10.1029/JA095iA04p03883.

J. E. Borovsky, Los Alamos National Laboratory, Mail Stop D466, Los Alamos, NM 87545, USA. (jborovsky@lanl.gov)

M. H. Denton, Physics Department, Lancaster University, Lancaster LA1 4WA, UK.